Kurdish Studies
August, 2024
Volume: 12, No: 5, pp 1481-1500
ISSN: 2051-4883 (Print) | ISSN 2051-4891 (Online)
www.KurdishStudies.net

DOI: 10.53555/ks.v12i5.3500

Numerical Simulation of Flow Characteristics Over Two Square Cylinders at Different Diameters with Various Gap Spacing

Shazia Kalsoom[1,2], Waqas Sarwar Abbasi[2,3], Raheela Manzoor[*1], Farida Aslam[4], Noreen Azhar[1]

[1*]Mathematics Department, Sardar Bahadur Khan Women's University, Quetta, Balochistan
[2]Mathematics Department, Air University, Islamabad, Pakistan.
[3]Department of Industrial Engineering Alma Mater Studiorum, Nasiriyah, 64001, Italy.
[4]Department of Mathematical Sciences, BUITEMS, Quetta 87300 Pakistan.

***Corresponding Author: Raheela Manzoor**
*E-mail: raheela_manzoor@yahoo.com

Abstract
Numerical simulations were conducted to investigate the effect of the upstream cylinder's size on flow characteristics and fluid force reduction. The study involved analyzing the flow around two consecutive, unequal-sized square cylinders arranged in tandem. The simulations utilized the Lattice Boltzmann method and covered various gap spacing's (g = s/d) ranging from 0.5 to 6. The Reynolds number was kept constant at Re = 150, while the diameter of the upstream cylinder varied among 20, 25, 30, 35, and 40. Prior to examining the effect of the cylinder diameter on flow at different spacing ratios, we assessed the computational domain and grid independence to determine the most accurate computational domain size and adequate grid points. Following this, we performed numerical simulations for different gap spacing's and cylinder diameters, and obtained results including vorticity and pressure contours, drag and lift coefficients, Strouhal numbers, and other physical parameters. The vorticity contour visualizations revealed distinct flow regimes based on their flow features, which were categorized as follows: i) Single bluff body flow regime (SBB), ii) Shear layer reattachment flow regime (SLR), iii) Steady flow regime (SF) and iv) Fully developed vortex shedding flow regime (FDVS). In terms of physical parameters, we calculated the mean drag coefficient (C_{dmean}), root mean square of drag (C_{drms}), lift coefficients (C_{lrms}), and Strouhal numbers (St) for both cylinders (C1 and C2). The highest mean drag coefficient was observed for the downstream cylinder (C2) at (D, g) = (25, 6), with a value of 1.6531. Similarly, the maximum numerical value of C_{drms} was recorded for C2 at (D, g) = (30, 6). Additionally, in some cases, the mean drag coefficient for the downstream cylinder showed negative values due to the thrust effect. Furthermore, due to the varying size of the upstream cylinder (C1) compared to the downstream cylinder (C2), S_t1 was greater than S_t2, with this trend observed at (D, g) = (40, 6).

Keywords: Gap Spacing, Reynolds Number, Lattice Boltzmann Method (LBM), Force Statistics, Diameter of cylinder.

1. Introduction

The study of flow past objects has garnered significant attention from engineers due to its impact on reducing fluid forces and suppressing vortex shedding in bluff bodies. These objects can take various shapes, such as square, circular, rectangular, and triangular, each of which has great significance in practical engineering fields like aerodynamics, hydrodynamics, and thermodynamics. Applications include the construction of bridges, high-rise buildings, micro-electromechanical systems, cooling devices, aircraft, submarines, and other vehicles. The flow around different body shapes with various characteristics presents distinct challenges. For example, square and rectangular objects typically have only two separation points, whereas circular objects can have more than two separation points, complicating the flow behavior. Much research has been conducted, either experimentally or numerically, to determine flow characteristics using single or multiple objects.

An experimental study conducted by Sakamoto et al. (1987) investigated the flow behavior of two square cylinders placed in the x-direction with a Reynolds number (Re) of 27,600 and observed significant changes in flow behavior. Chiu and Ko (1995) performed an experimental study with two square cylinders of unequal sizes and found bistable flow in the gap spacing range of $1.12 \leq g \leq 2$. Ko et al. (1996) conducted numerical simulations to investigate induced fluid forces and vortex shedding suppression using two side-by-side circular cylinders with a size ratio of 2:1. Their results indicated that the greatest pressure on the smaller cylinder could signify a separation point known as the point of inflection. Zhang and Zhou (2001) experimentally studied the flow past three cylinders of equal and unequal sizes with different gap spacings, employing techniques such as hot-wire and laser Doppler anemometry. They discussed the effect of gap spacing on flow behavior for unequal-sized cylinders. Dalton et al. (2001) performed numerical investigations using two cylinders of different sizes, with a small control cylinder placed near the main square cylinder, across Reynolds numbers of 100, 1,000, and 3,000. They found that fluid forces decreased around the small control cylinder at larger gap spacings. Kang (2003) studied the side-by-side arrangement of two cylinders at Re = 40–160 and $g < 5$ using an immersed boundary condition. He found that gap spacing significantly influenced flow behavior compared to Reynolds number. Agarwal et al. (2006) conducted numerical simulations using the SRT-LBM method at Re = 73 and identified two flow regimes, noting that flow transition occurred at larger gap spacings. Le and Yang (2009) studied flow phenomena with two square cylinders of the same size at Re = 160 and identified

four types of flow regimes. They observed that vortex shedding increased due to the presence of a separation point related to gap spacing. Gao et al. (2010) numerically studied the flow past two unequal-sized circular cylinders in a side-by-side arrangement at Re = 300 and found various flow regimes due to vortex shedding. Yen and Liu (2011) conducted experiments with two side-by-side square cylinders at spacing ranges of $0 \leq g \leq 12$ and Re values between 2,262 and 28,000, investigating three flow regimes. Sohankar (2012) performed a numerical study of flow across two square cylinders with Re ranging from 130 to 1,000 and identified three flow regimes. They noted that three-dimensional effects were delayed when Re exceeded 200. Manzoor et al. (2016) conducted numerical simulations for flow past two equal-sized square cylinders and found that, at certain spacings, the downstream cylinder experienced higher fluid forces compared to the upstream cylinder due to turbulent flow behavior. Luo and Gan (2016) investigated flow structure mechanisms past two inline circular cylinders with a diameter ratio of 0.33. They found shear layer reattachment with the downstream cylinder at small gap spacings, leading to complete separation of the cylinders. At larger gap spacings, both cylinders generated shed vortices. Islam et al. (2017) computationally studied the flow around three cylinders of unequal size arranged side-by-side at Re = 160 with gap spacings ranging from $0.5 \leq g \leq 5$. They observed changes in flow regimes depending on the configuration of the three side-by-side cylinders, noting that the drag coefficient was highest for the smallest cylinder across all configurations. Waqas et al. (2018) examined the flow states for two square cylinders in an inline arrangement with Re ranging from 1 to 130 and gap spacings of g = 2 and 5. They found maximum drag reduction at g = 2 and Re = 1 compared to g = 5. Ghazala et al. (2019) performed numerical investigations of flow across two square cylinders arranged in a staggered configuration at Re = 160 and studied the effect of gap spacing, identifying five flow regimes. Skonecki and Buick (2023) investigated the flow around two circular cylinders in tandem, staggered, and side-by-side arrangements at Re = 3,900, finding that the tandem arrangement was more sensitive and that three types of flow regimes existed in the staggered arrangement at this Reynolds number. Manzoor et al. (2024) conducted numerical simulations for flow around three cylinders of different sizes with Re ranging from 120 to 200 and gap spacings varying from 1 to 6. They observed four different types of flow regimes and found the maximum mean drag coefficient for the first cylinder (C1) at (Re, g) = (200, 3), where the flow regime was SLR.

From the reviewed literature, it is evident that most researchers have focused on objects of the same diameter, regardless of shape, with less attention given to the effects of varying diameters on fluid force reduction and vortex shedding suppression. Therefore, the present study aims to investigate the effect of different upstream cylinder sizes on the downstream cylinder to reduce fluid forces at various gap spacings, using a fixed Reynolds number of Re = 150.

In present problem, we discussed literature review, statement of problem, boundary conditions, study of computational domain and grid independence study, finally we discussed results and discussion along conclusions in different sections.

2. Problem Description with Boundary Condition along Physical Parameters:

Numerical simulations are conducted for flow behind two unequal sized square cylinders in two-dimensional (2D) computational domain that is illustrated in Fig 1. In this study incompressible, viscous, steady flow with uniform inflow velocity U_∞ is considered. The size of past upstream cylinder denoted by D is varied in between from D = 20 – 40 with fixed size (d) of downstream cylinder d = 20, respectively. The gaps spacing between the cylinders $C_1$and C_2 varies from g = 0.5 to 6 at fixed Reynolds number Re = 150. The up-streams distance is selected at L_u = 8d, downstream distance is L_d = 24d and height of channel is H= 16d for present problem. At inlet position, uniform inflow velocity ($u = U_\infty$, $v = 0$) is applied and convective boundary condition is applied at outlet region of the channel ($\frac{\partial u}{\partial x} = 0, v = 0$) (Guo et al. 2008) Since the walls of the channel and cylinders are no more rotating and in stationary

position, therefore no – slip boundary condition is prescribed at upper and lower walls of channel and both the cylinders (Zhou et al. 2008). As the flow is uniform distributed, due to which induce forces are exerted uniformly on channel and for the calculation of forces momentum exchange method is applied on the surface of the computational domain (Dazhi et al. 2003).

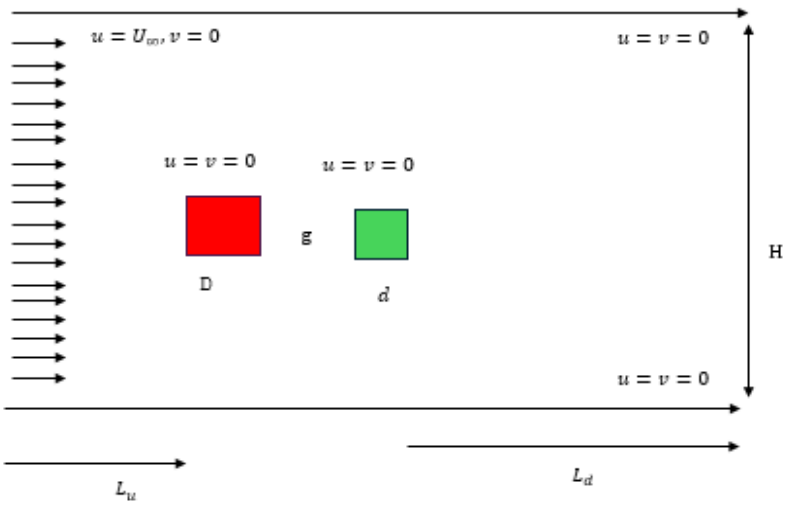

Fig. 1 Systematic Flow Configuration Past Un-Equal Size Cylinder at Re = 150.

In this study some physical parameters such as gap spacing, drag and lift coefficients, mean drag coefficient, root mean square values of drag and lift coefficients, Strouhal number are used and defined as

$$\text{Reynolds number} = \text{Re} = \frac{U_\infty d}{\nu} \quad (1)$$

$$\text{Drag coefficient} = C_d = \frac{2F_d}{\rho U_\infty^2} \quad (2)$$

$$\text{Lift coefficient} = C_l = \frac{2F_L}{\rho U_\infty^2} \quad (3)$$

$$\text{Strouhal number} = St = \frac{f_s d}{U_\infty} \quad (4)$$

$$\text{Root mean square of drag coefficient} = C_{drms} = \sqrt{\sum_{t=1}^{n}(C_d(t) - \text{mean}\,(C_d(t)^2)/n} \quad (5)$$

$$\text{Root mean square of lift coefficient} = C_{lrms} = \sqrt{\sum_{t=1}^{n}(C_l(t) - \text{mean}\,(C_l(t)^2)/n} \quad (6)$$

Where f_s is the vortex shedding frequency, ρ is the density of fluid and n is the number of time steps.3.

3. Lattice Boltzmann Method:

The Lattice Boltzmann method (LBM) is a two-dimensional numerical technique which has performed a vital and tremendous role in computational fluid dynamics (CFD). It provided a strong versatile technique for fluid dynamic problems, and it can be easily applied to resolve the problem associated with the multi directional flows, complex geometries and to recover the Navier Stokes equation (Sukop and Thorn (2007).It is explicit and conditionally stable and provides good stability as compared to other numerical methods (Wolf- Gladrow, 2009). Another application is the derivation of equation of state for pressure instead of solving poison's equation (Mohammad (2011). It consists of two main processes, i) streaming and ii) collision and is based on mesoscopic scale which is a bridge between micro scale and macro scale. The main concept and idea have been taken from Lattice Gas Cellular Automata (LGCA) (Mohammad, 2011). In the current study governing differential equation for an incompressible, unsteady and uniform flow is Cowling considered a

$$\nabla . u = 0 \quad (7)$$

$$\frac{\partial u}{\partial t} + (u.\nabla)u = -\frac{1}{\rho}\nabla P + \vartheta \nabla^2 u \quad (8)$$

Where ϑ is kinematics viscosity. Eq. (7) is representing the continuity equation and Eq. (8) is the momentum equation. The Lattice Boltzmann equation in general form is follow as (Wolf-Gladrow, 2009).

$$\frac{\partial \lambda}{\partial t} + e.\nabla\lambda = -\frac{1}{\tau}\left(\lambda_i - \lambda_i^{eq}\right) \quad (9)$$

Equations (7 & 8) can be recovered by using the Chapman Enskog expansion (Chapman and Cawling (1970)) in terms of discretized form of Lattice Boltzmann equation as given as

$$\lambda_i(x + \Delta x, t + \Delta t) - \lambda_i(x,t) = -\frac{\nabla t}{\tau}\left(\lambda_i(x,t) - \lambda_i^{eq}(x,t)\right) \quad (10)$$

In the above two equations λ_i and λ_i^{eq} are representing the density distribution and equilibrium density distribution function for Lattice Boltzmann method at position $\mathbf{x}$ and time $\mathbf{t}$. While τ is relaxation time having values within the range of $0.5 < \tau < 2$. Right hand-side in equation (10) shows the collision process in which particles collide and left-hand side is the streaming process where the particles propagate to near adjacent node. The equilibrium distribution function is defined as follows

$$\lambda_i^{eq} = \rho\varpi_i\left(1 + \frac{e_i.u}{c_s^2} + \frac{(e_i.u)^2}{2c_s^4} - \frac{1}{2c_s^2}u^2\right) \quad (11)$$

Here ϖ_i are presenting the weighting coefficients in equation (11) and having different values for different models implemented in LBM. In this study we used two-dimensional nine velocity particles (D_2Q_9) model (see Fig 2) and its values are defined in equation (12)

$$\varpi_i = \begin{cases} \frac{4}{9} & i = 0 \\ \frac{1}{9} & i = 1,2,3,4 \\ \frac{1}{36} & i = 5,6,7,8 \end{cases} \quad (12)$$

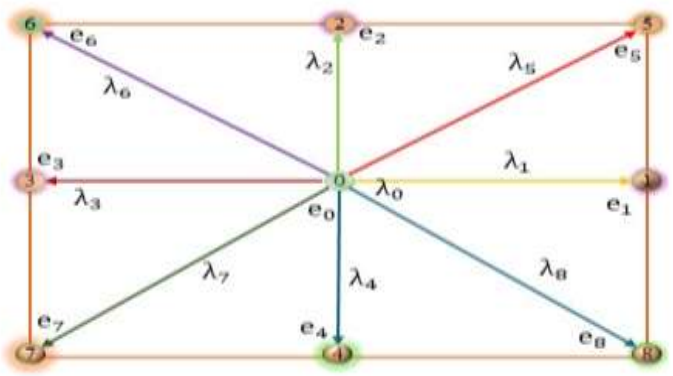

Fig 2. Lattice structure for D2Q9 model.

The density and velocity of particle are follow as;

$$\rho = \sum_{i=0}^{8} \lambda_i \tag{13}$$

$$u = \frac{1}{\rho}\sum_{i=0}^{8} e_i \lambda_i \tag{14}$$

Where ρ is the density and u is the velocity of the medium.
The kinematics viscosity and pressure are computed as.

$$\vartheta = c_s^2 \delta t \left(\tau - \frac{1}{2}\right) \tag{15}$$

$$p = \rho c_s^2 \tag{16}$$

Here, c_s^2 is speed of sound and its value is 1/3 for D2Q9 model.

4. Effect of Computational domain and Grid Independence Study

4.1 Effect of Computational Domain:

Two-dimensional numerical simulation is performed through Lattice Boltzmann Method for flow past two unequal sized square cylinders in longitudinal position to study the effect of computational domain at fixed value of Re = 150 in order to select an appropriate computational domain. The different values of L_u, L_d and H are selected, and we calculated the values of physical parameters at these selected values of computational domain as shown in Table 1. In case IV, the mean drag coefficients for both cylinders C1 represents maximum magnitude and minimum value is found in case VIII as compared to other selected cases. It is observed that case I, II, III and VI having similar values of mean drag coefficients for both selected cylinders. If we compared the values of other two physical parameters, such as root mean square values of drag coefficients and Strouhal numbers for C1 and C2, similar behavior is observed like C_{dmean}. So, we selected the case (VI) L_u = 7d, L_d = 16d and H = 16d for performing all simulations of current study.

Table1. Effect of computational domain at Re = 150, D = 30 & g = 2d.

Cases	**L_u ; L_d ; H**	**$C_{dmean}1$**	**$C_{dmean}2$**	**$C_{drms}1$**	**$C_{drms}2$**	**S_t1**	**S_t2**
I	L_u = 7d; L_d = 14d; H = 16d	1.3828	-0.2219	0.4130	0.3580	0.1459	0.0987
II	L_u = 7d ; L_d = 18d; H = 16d	1.3829	-0.2220	0.4096	0.3571	0.1459	0.0987
III	L_u = 7d ; L_d = 20d; H = 16d	1.3828	-0.2219	0.4130	0.3580	0.1459	0.0987
IV	L_u = 5d; L_d = 16d; H = 16d	1.4733	-0.2339	0.4141	0.3634	0.1526	0.1037
V	Lu = 6d; L_d = 16d; H = 16d	1.4173	-0.2267	0.4070	0.3572	0.1459	0.0987
VI	L_u = 7d; L_d = 16d; H = 16d	1.3829	-0.2218	0.4122	0.3523	0.1442	0.0987
VII	L_u = 8d; L_d = 16d; H = 16d	1.3617	-0.2194	0.4092	0.3484	0.1459	0.0953
VIII	L_u = 9d; L_d = 16d; H = 16d	1.3470	-0.2167	0.4098	0.3534	0.1425	0.0953
IX	L_u = 7d; L_d = 16d; H = 14D	1.4098	-0.2300	0.4162	0.3537	0.1459	0.0987
X	L_u = 7d; L_d = 16d ; H = 15d	1.3945	-0.2252	0.4140	0.3571	0.1459	0.0987
XI	L_u = 7d; L_d = 16d; H = 17d	1.3741	-0.2195	0.4127	0.3542	0.1459	0.0970
XII	L_u = 7d; L_d = 16d; H = 18d	1.3664	-0.2167	0.4123	0.3555	0.1442	0.0987

4.2. Grid independence study

Table 2. Grid points study for flow around a single square cylinder at fixed Re = 150.

Grid-points	C_{dmean}	C_{drms}	C_{lrms}	S_t
d1 = 10; g =1d	1.4507	0.2764	0.3101	0.1484
d1 = 16; g = 1d	1.3971	0.3260	0.2725	0.1532
d 1= 20; g = 1d	1.3754	0.3558	0.2490	0.1545
d1 = 24; g = 1d	1.3612	0.3833	0.2337	0.1569
d1 = 30; g = 1d	1.2729	0.6212	0.1371	0.1581

For selection of an appropriate grid points, we conducted numerical study by selected different grid points 10, 16, 20, 24 & 30 and calculated the values physical parameters and represented in Table 2. The values of C_{dmean}, C_{drms}, C_{lrms} and S_t. The value of mean drag coefficient is least at d1 = 30 and largest value is found at d1 = 10. The values of C_{dmean} at d1 = 16, 20 & 24 are approximately. Similar behavior is observed for all other physical parameters. Therefore, we will select d1 = 20 for conducting all the simulations for present problem. Guo et al. (2009) also selected d1 = 20 for her research work. For code validation, we can check out previous papers Hamid et al. (2019), Manzoor et al. (2016), Islam et al. (2017) etc.

5. Results and Discussions

A two-dimensional numerical simulation of flow past two inline square cylinders of unequal size is conducted through numerical technique of Lattice Boltzmann Method. The value of the Reynolds number is fixed at Re = 150 and gap spacing between the cylinders varies from g = 0.5 to 6. The size of upstream cylinder is varied from D = 20 – 40 to study the flow characteristics at unequal sizes of cylinder by varying the spacing ratio. The results are exhibited and discussed in the form of Vorticity contour, Pressure contour, Strouhal number, Time history analysis of drag and lift coefficients, and force coefficients.

To make the study simple, only a few results are presented, and results of similar behavior are avoided to present here. In the Vorticity contour visualization solid lines represent the positive vortices, and dashed lines represent the negative vortices. While in Pressure contour visualization dark red color indicates maximum pressure and light red color represents minimum pressure but positive values. Similarly, green and blue colors represent negative values of pressure and have negligible impact on the computational domain.

In Vorticity contour visualization, four different types of flow behavior are observed at different values of gap spacing and size of cylinder. Those flow behaviors are categorized as i) Single bluff body flow regime (SBB), ii) Share layer reattachment flow regime (SLR), iii) Steady flow regime (SF) and iv) Fully developed vortex shedding flow regime (FDVS). Those flow regimes are discussed below.

i) Single bluff body flow regime (SBB)

When the gap spacing between two cylinders (C1 & C2) is small, the flow behavior resembles that of a single bluff body. This flow regime is typically observed when the diameter ratio D is between 20 to 35 and the gap spacing g is between 0.5 to 1.5. The vorticity contour graphs for this flow mode are depicted in Fig 3 (a-c). When the upstream flow impacts the upper and lower corners of the upstream cylinder, some of the flow hits the up and down wake regions of the downstream cylinder. Due to the small gap spacing, there is no flow observed between the gaps of both cylinders (C1 & C2). In the upper and lower wake regions of the downstream cylinder, vortex rolls form and transform into alternate vortex shedding, representing the Von Kármán vortex street, which is typically seen in the flow behind a single cylinder. This pattern is also observed in the studies by Ahmed et al. (2021) and Bao et al. (2010) for flow past two tandem square cylinders. Fig 3 (d-f) illustrates the pressure variations in the wake and surrounding regions of both unequal-sized cylinders in the single bluff body flow regime at specific sizes of C1 and gap spacing between C1 and C2. Pressure has a significant impact on the induced forces. The maximum pressure occurs at the sharp corners of the front surface of the upstream cylinder, represented by a bloody red color. However, the pressure drops to negative in the gap between the upstream and downstream cylinders, indicated by a green color, due to the absence of flow between C1 and C2. The pressure contour graphs show negative and lower pressure values in the wake behind the downstream cylinder. Alternate vortex shedding in the wake region behind the downstream cylinder causes the pressure to become negative and approximately uniform throughout the computational zone (see Fig 3 (d-f)). The temporal variation of drag and lift coefficients for this flow regime is shown in Fig 3 (d-f) and Fig 3 (g-i). From Fig 3 (g-i), it is evident that the drag coefficient of the upstream cylinder (C_d1) remains constant and stable due to the absence of flow between the cylinders C1 and C2. The drag coefficients of the downstream cylinder (C_d2) exhibit periodic behavior with a small amplitude, indicating vortex generation in the wake region of C2. Similarly, the lift coefficients of time analysis show a sinusoidal behavior for both the cylinders C1 and C2. The amplitude of the lift coefficients for the downstream cylinder (C_l2) is greater than that of the upstream cylinder (C_l1), attributed to vortex generation behind the wake region of the downstream cylinder. These observations provide insights into the complex interactions and flow dynamics between two cylinders at small gap spacing, which is crucial for various engineering applications. The power spectrum's plot for the single bluff body flow is shown in Fig 3 (j, k, and l). A single sharp primary peak is observed for this flow pattern. No secondary peak is noted here due to regular vortex shedding. The amplitude of Strouhal number for C1 is larger than that of C2. This phenomenon was also exhibited by Hamid et al [2019].

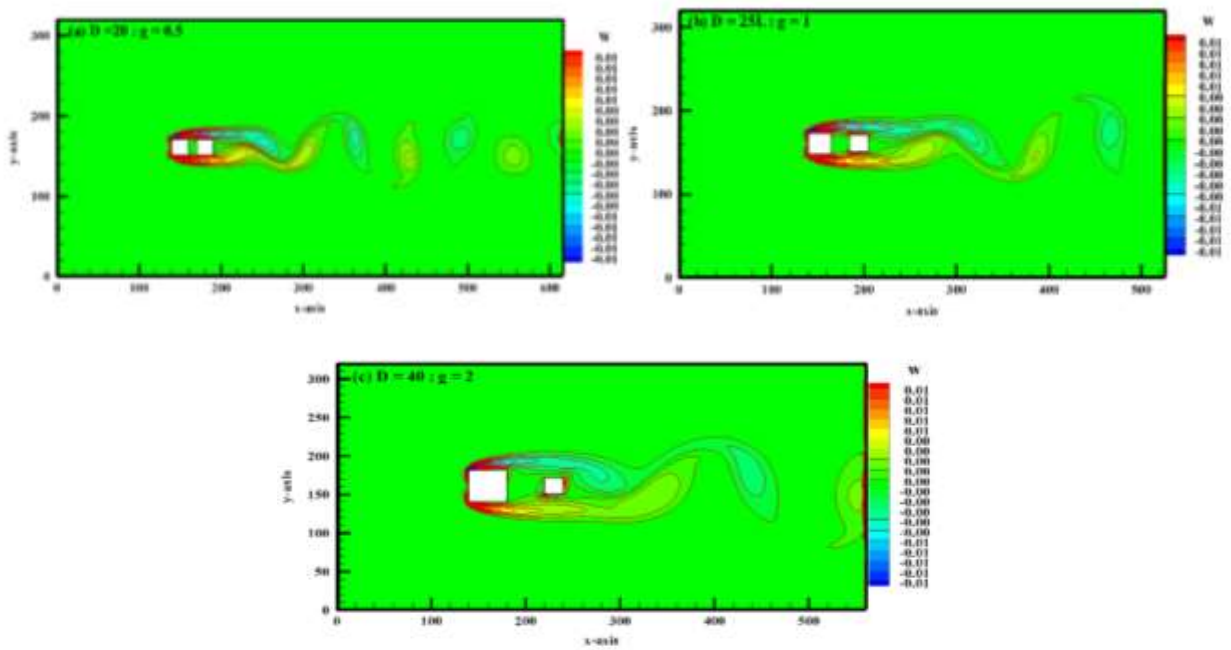

Fig 3 (a-c). Vorticity contour visualization for SBB flow regime at Re = 150.

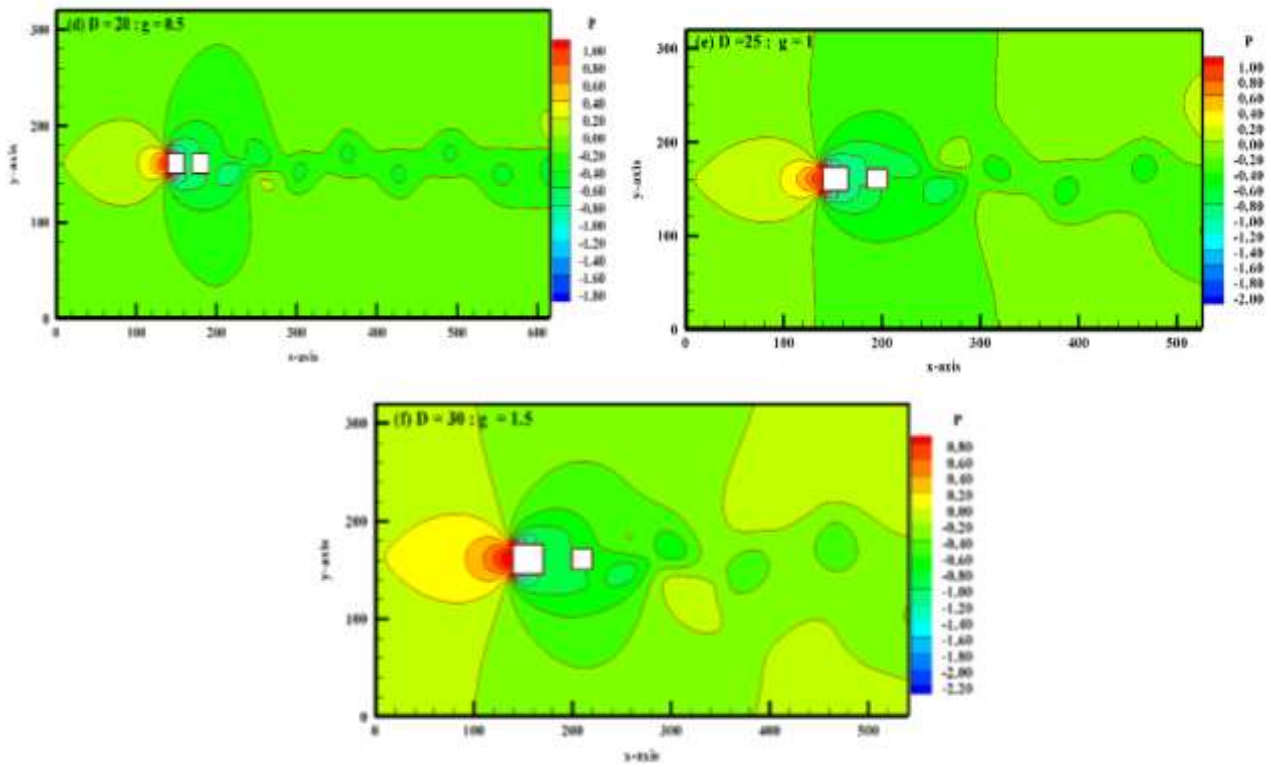

Fig. 3 (d-f). Pressure contour visualization for SBB flow regime at Re = 150.

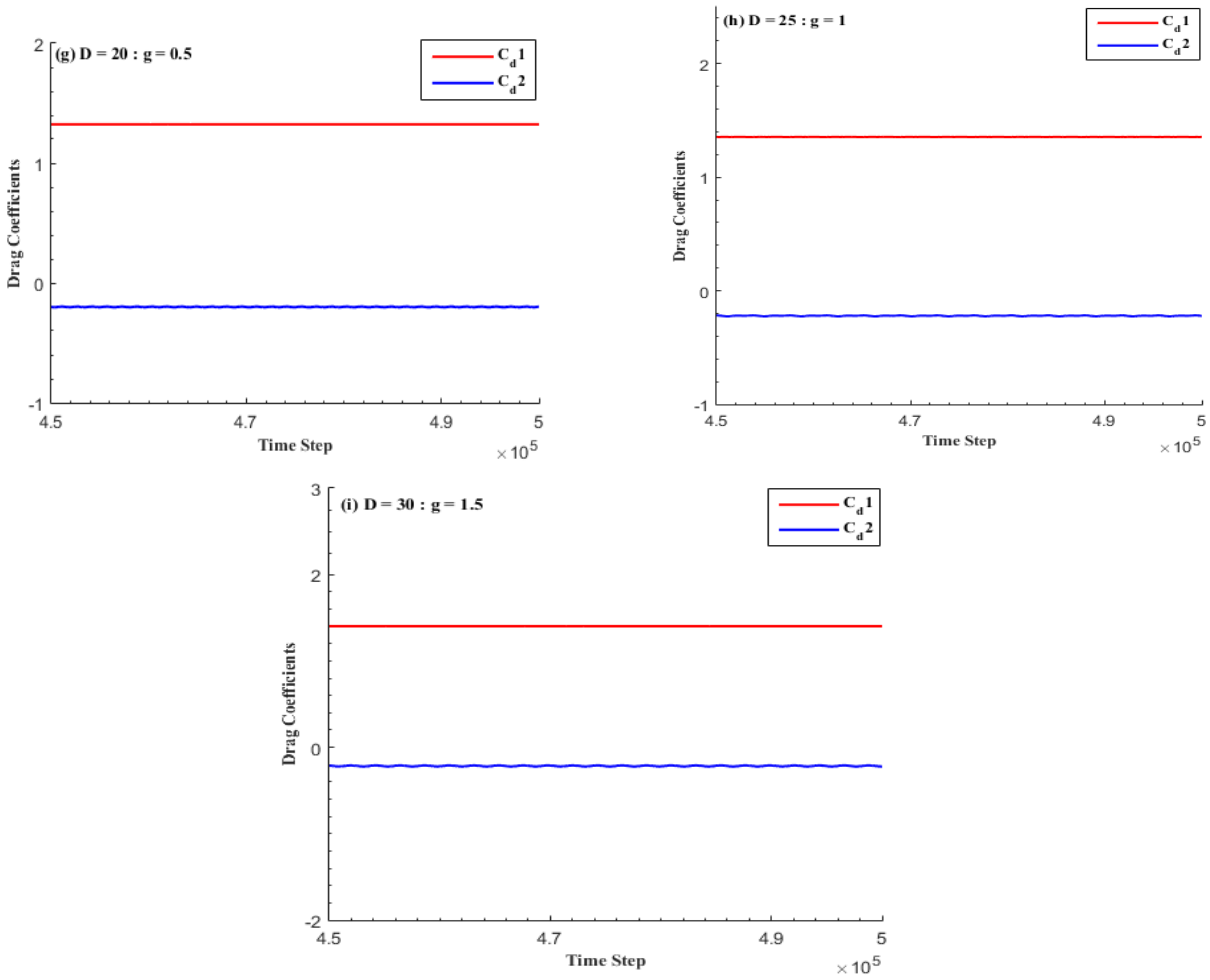

Fig 3 (g-i). Drag Coefficients for SBB flow regime at Re = 150.

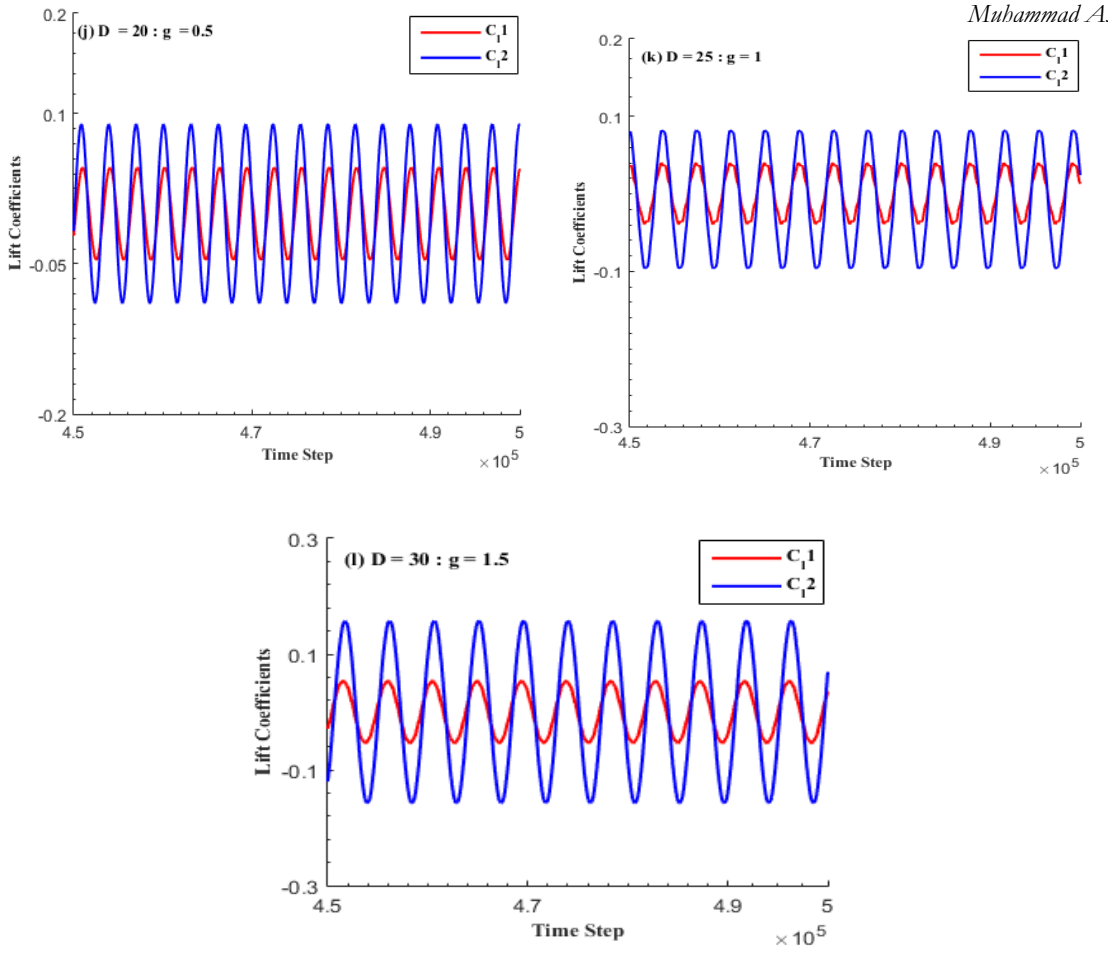

Fig 3 (j-l). Lift Coefficients for SBB flow regime at Re = 150

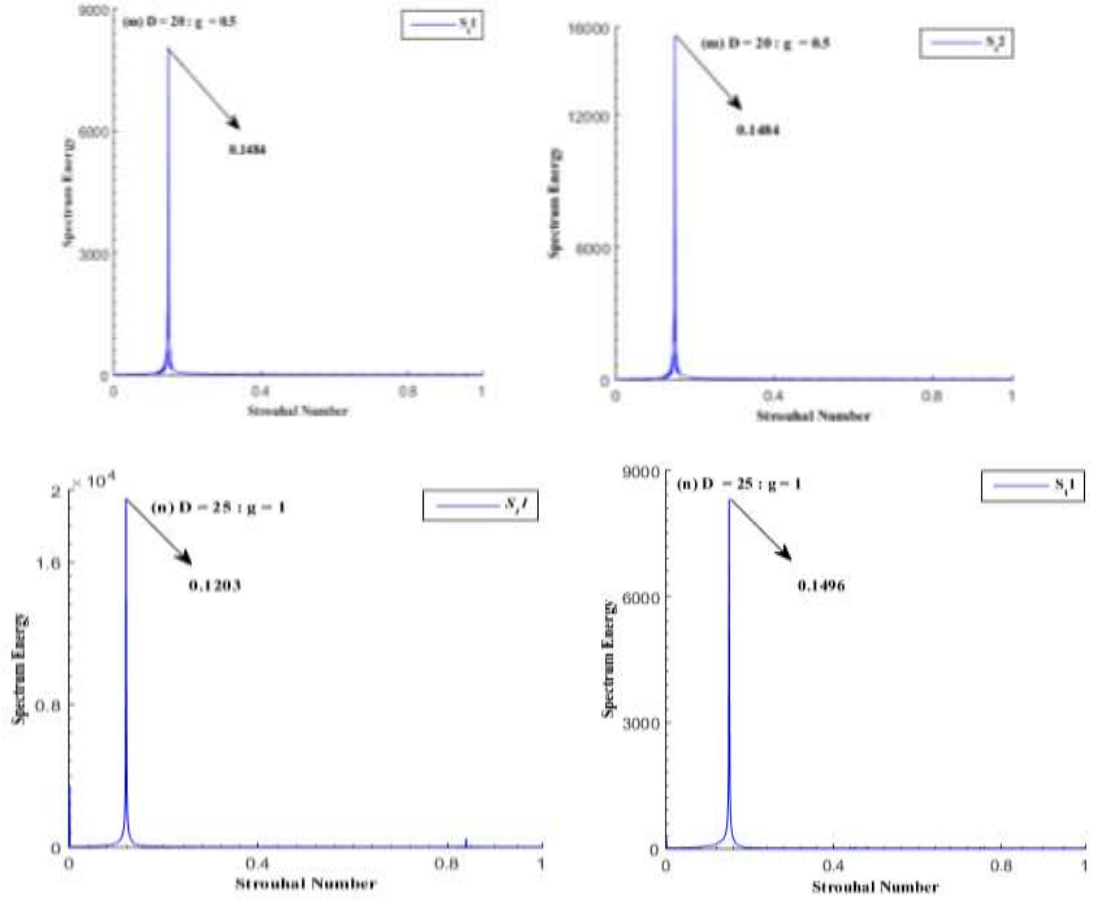

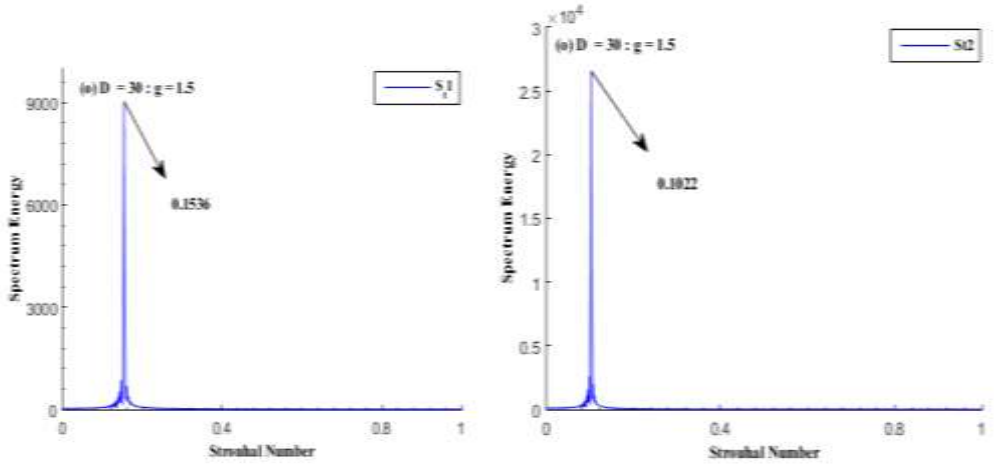

.Fig 3 (m-o). Strouhal number for SBB flow regime at Re = 150

ii) Share layer reattachment flow regime (SLR)

The second existing flow regime is shear layer reattachment flow. This behavior of flow occurs at characteristic sizes of the upstream cylinder varying from (D, g) = (20, 2), (20, 2.5), (20, 4), (25, 2), (25, 2.5), (25, 3), (25, 4), (30, 2), (30, 2.5), (30, 3), (30, 4), (35, 2), (35, 2.5), (35, 3), (35, 4), (40, 0.5), (40, 1), (40, 1.5), (40, 2), (40, 2.5), (40, 3), (40, 4) and (40, 5), respectively. To demonstrate this flow regime, some selected cases of vorticity are considered here and shown in Fig. 3 (a-c). When the upcoming flow hits the upper and lower edges of the upstream cylinder, it separates into the upper and lower wake regions of C1, where the shear layer reattaches to C2. Since no flow is observed in the gap between C1 and C2, the wake behind the downstream region rolls up, indicating the mechanism of vortex generation in the middle of the downstream computational domain. It is noted that vortex shedding occurs far away from the wake behind the downstream region as the gap increases. By observing the second flow regime (see Fig. 4), it is revealed that pressure modifications occur in the near-wake region and surroundings of both the unequal-sized cylinders C1 and C2. In this regime, the highest pressure is observed at the front surface of the upstream cylinder C1, but it turns negative at the back corners. The blue color between the gap of the two square cylinders C1 and C2 indicates the lowest and negative pressure values where no flow exists. By observation, it is revealed that the distribution pressure undergoes variations with negative values caused by the effect of shear layers. It is noted that the pressure distribution is not uniform throughout the channel. The drag and lift coefficients for this flow pattern are presented in Fig. 4 (d-f). It is observed that the drag coefficients for both cylinders C1 and C2 is constant at (d, g) = (20, 2), (20, 2.5), which occurs due to the formation of vortex shedding far away from the downstream of the channel. For D = 25-35 with g = 2 – 4 and D = 40 along with g = 0.5 – 5 where C_d1 is stable while C_d2 represents periodic behavior with a small magnitude. For this flow regime, lift coefficient graphs are shown in Fig. 4 (g-i). The lift coefficients graphs exhibit sinusoidal behavior, where the amplitude of C_l2 is greater as compared to C_l1. This is attributed to the vortex shedding mechanism from both cylinders. The power spectrum plot for this flow mode is shown in Fig. 4 (g-i). At (d, g) = (20, 2), and (20, 2.5), spectrum energy graphs represent a wide and long primary peak, with no secondary peak found. The wider primary peak is due to the formation of vortices far away from the downstream wake region at middle values of g between C1 and C2. Due to the same size of both cylinders, the amplitude of the energy spectrum of both cylinders is identical. At (D, g) = (20, 4), (25,1.5), (25, 2), (25, 2.5), (25 ,3), (25, 4), (D, g), (35, 2.5) and (35, 3), the Strouhal graph shows a sharp long primary peak along with a minor single secondary peak. Similarly, at (D = 30 & 40 along with g = 1.5 – 4 and (D, g) = (35, 1.5), (35, 2), (35, 4), the power spectrum's plot exhibits a prominent long primary peak as well as minor secondary peaks. It is noted that the magnitude of the Strouhal number for C1 is greater than for C2 due to the unequal size of both cylinders in all cases except when the cylinders are of equal size.

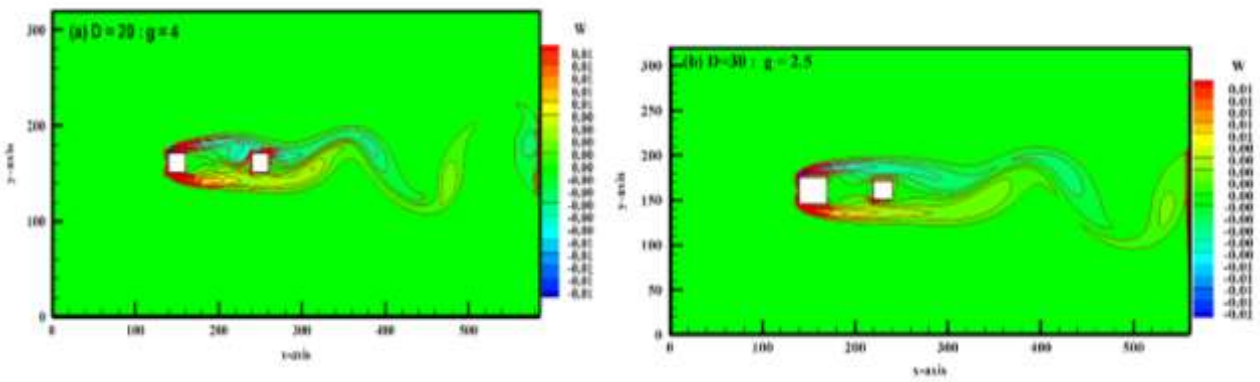

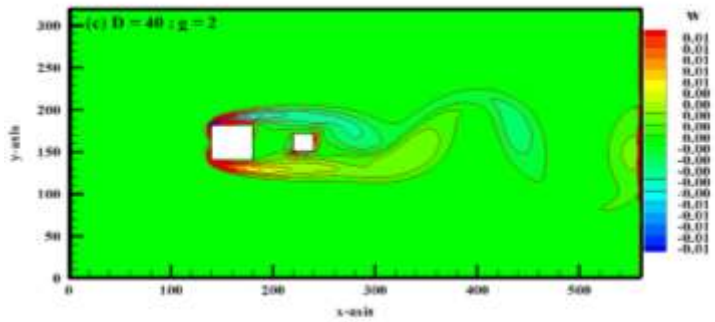

Fig. 4 (a-c). Vorticity contour R flow visualization for SLR flow regime at Re = 150.

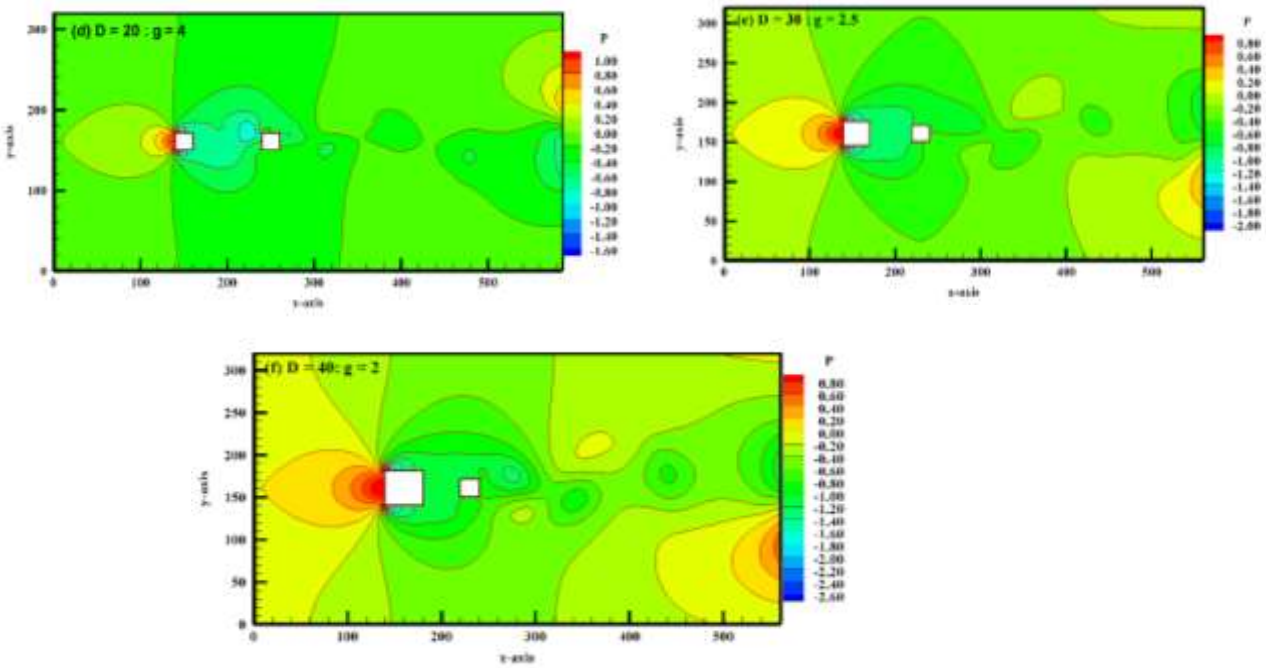

Fig 4 (d-f). Pressure contour R flow visualization for SLR flow regime at Re = 150

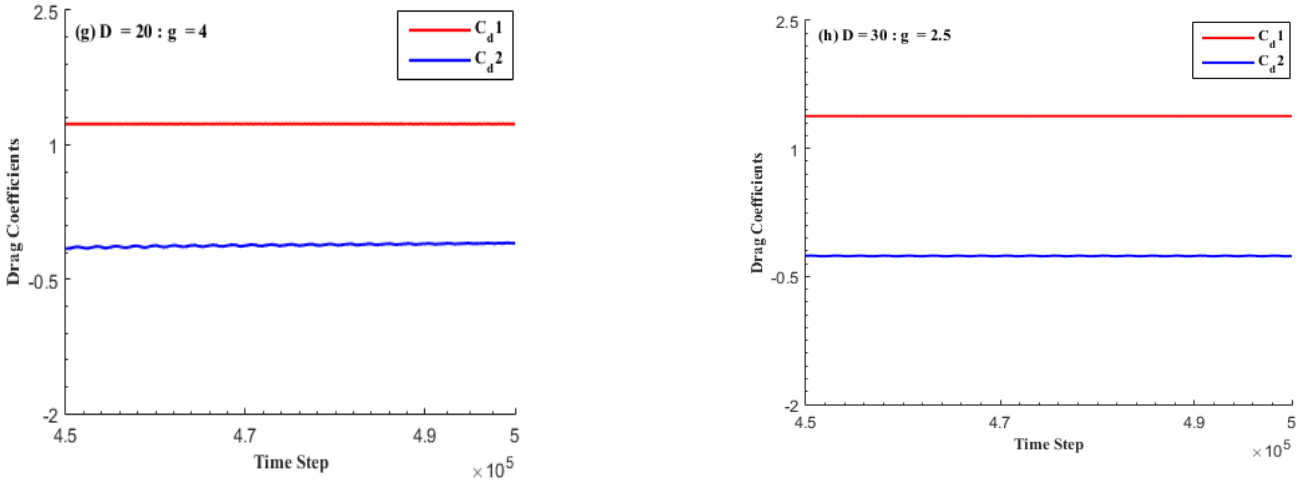

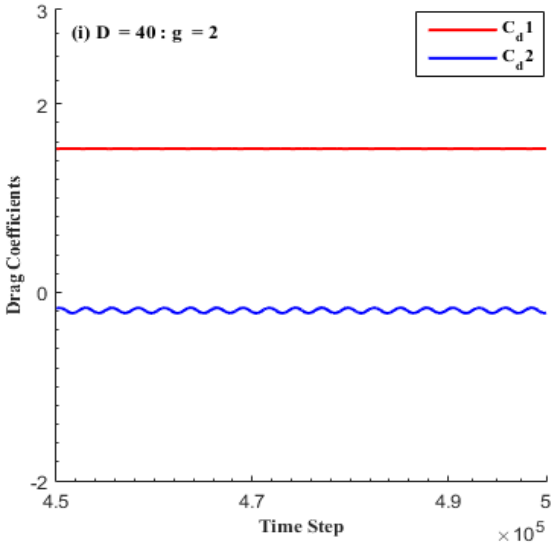

Fig 4 (g-i). Drag Coefficient for SLR flow regime at Re = 150.

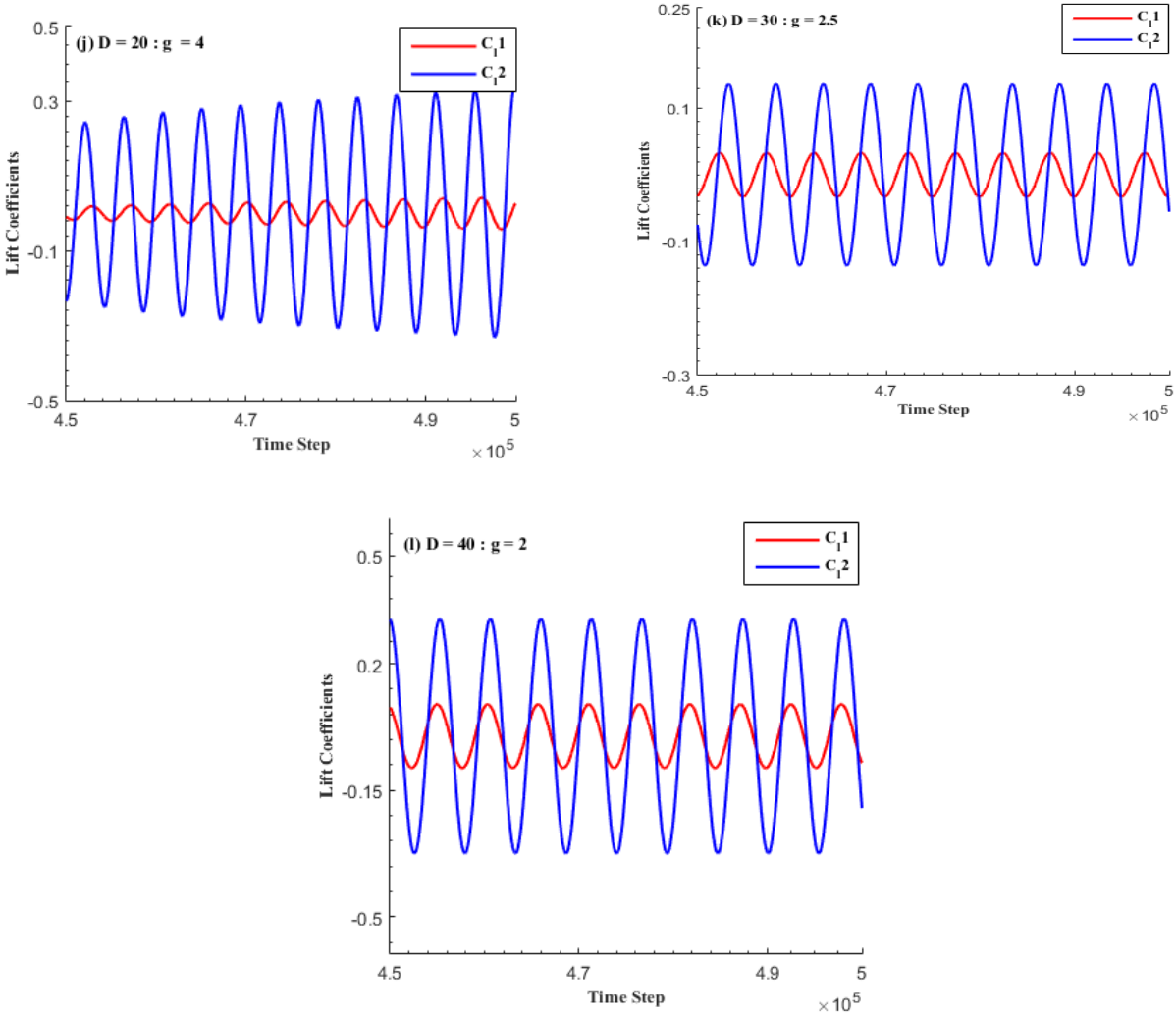

Fig 4 (j-l). Lift Coefficient for SLR flow regime at Re = 150

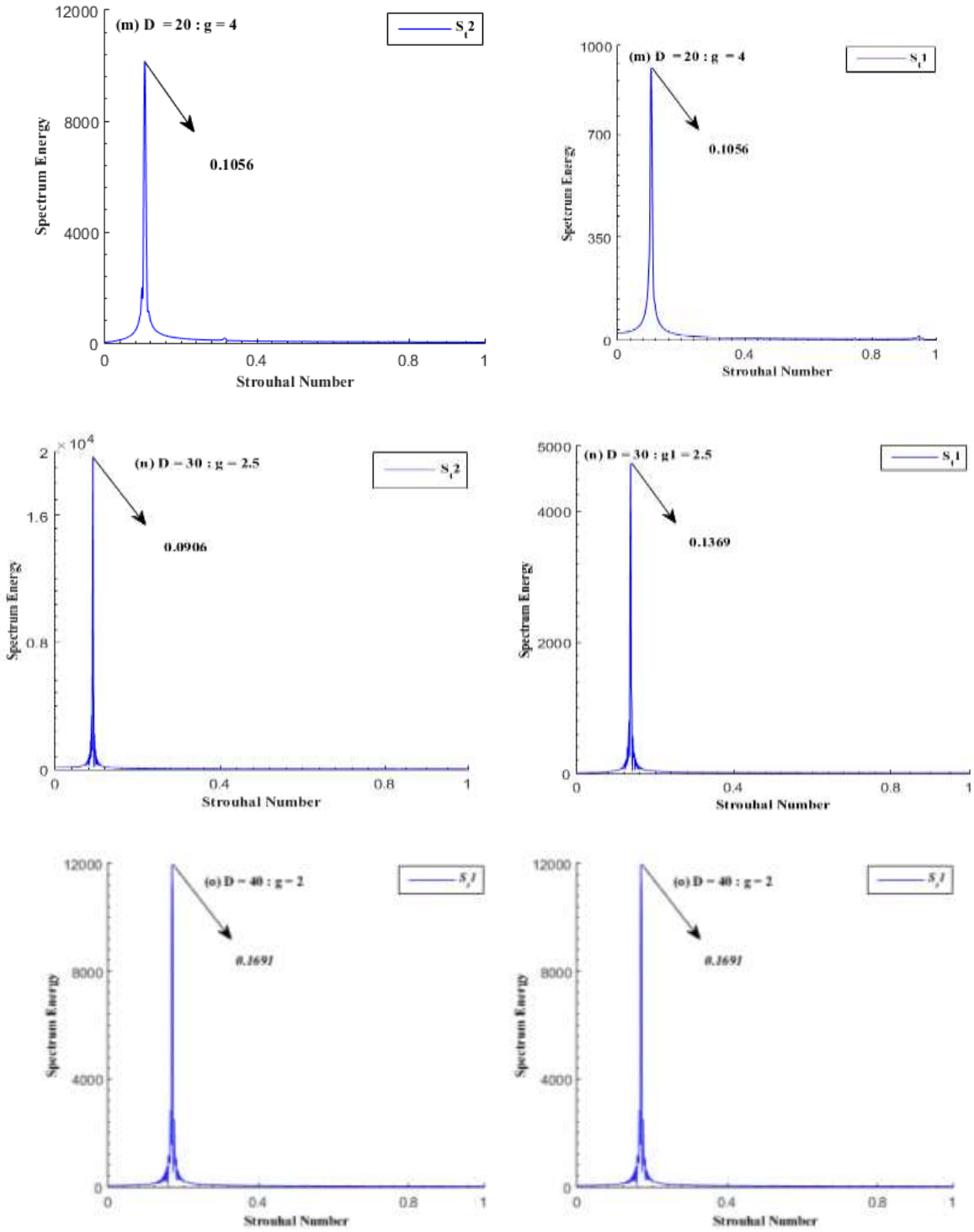

Fig 4 (m-o). Strouhal number for SLR flow regime at Re = 150.

iii) Steady flow regime (SF)

The third observed flow regime is the steady flow (SF) regime. In the current study, this flow exists in the downstream cylinder C2 at (D, g) = (20, 3) (see Fig 5). To discuss this flow regime, only one case of the vorticity contour graph is shown in Fig 5 (a). There is no observed flow in the gap spacing between the upstream and downstream cylinders. In this vorticity plot, the dashed lines represent negative vorticity, and the solid lines represent positive vorticity generated from the lower edges of the cylinder. The flow is stable here, so it does not merge in the gap. Instead, the flow is slightly suppressed inside from the upper and lower corners of both cylinders C1 and C2. As a result, the generation mechanism of vorticity does not occur throughout the computational domain. The same flow mode is observed in the study done by Manzoor et al. [2023], Islam et al. [2019] and Boa et al. [2012], which also described a similar phenomenon. Regarding pressure distribution, the greatest pressure, like the previous case, occurs at the front side of the upstream cylinder C1 (see Fig 5 (b)). The blue color represents the lowest and negligible impact of pressure with negative values in the gap between the upstream and downstream cylinders due to the absence of flow between C1 and C2. The pressure distribution mostly shows negative values throughout the domain, except near the wake region of the upstream cylinder (see Fig 5 (b)), due to the steady flow. The time analysis of drag and lift

coefficients for this flow characteristic is illustrated in Fig 5 (c, d), providing a vivid consideration of this tendency. The drag and lift coefficients graphs for both cylinders C1 and C2 show a straight line and stability at (D, g) = (20, 3) due to the steady flow and the absence of vorticity formation in the whole channel. The energy spectrum analysis lift coefficient plot for this steady flow regime is exhibited in Fig 5 (e). Due to the absence of vortex shedding in the entire computational zone for this flow pattern, there is no difference in the drag and lift coefficient plots, showing the same stable behavior. The graph clearly indicates that no energy spectrum exists due to the steady flow, and no formation of vorticity is observed.

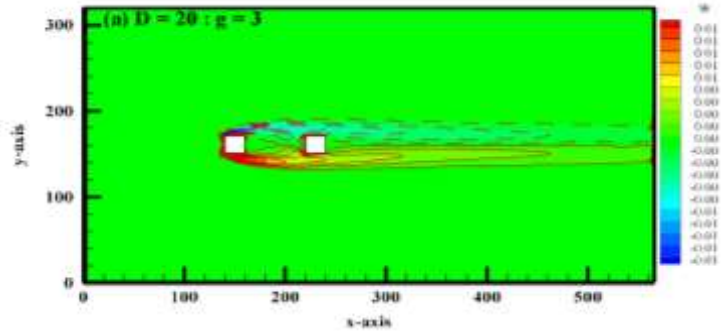

Fig 5 (a). Vorticity contour visualization for SF flow regime at Re = 150

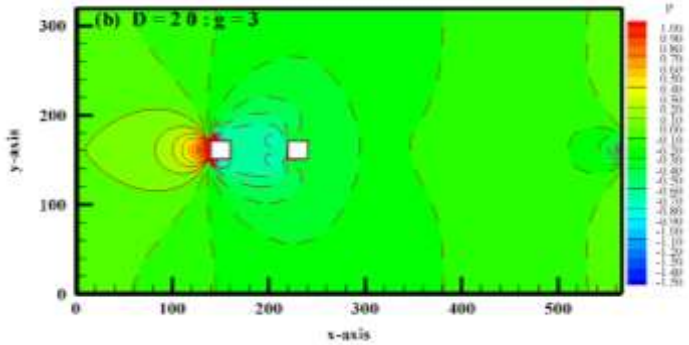

Fig 5(b). Pressure contour visualization for SF flow regime at Re = 150

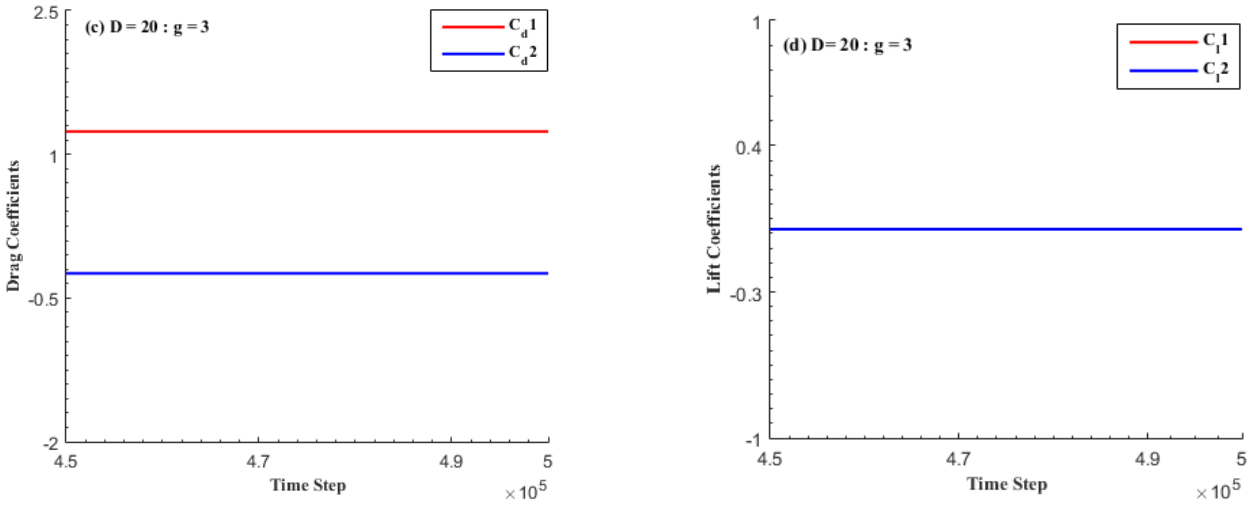

Fig 5 (c, d) Drag and Lift Coefficient for SF flow regime at Re = 150

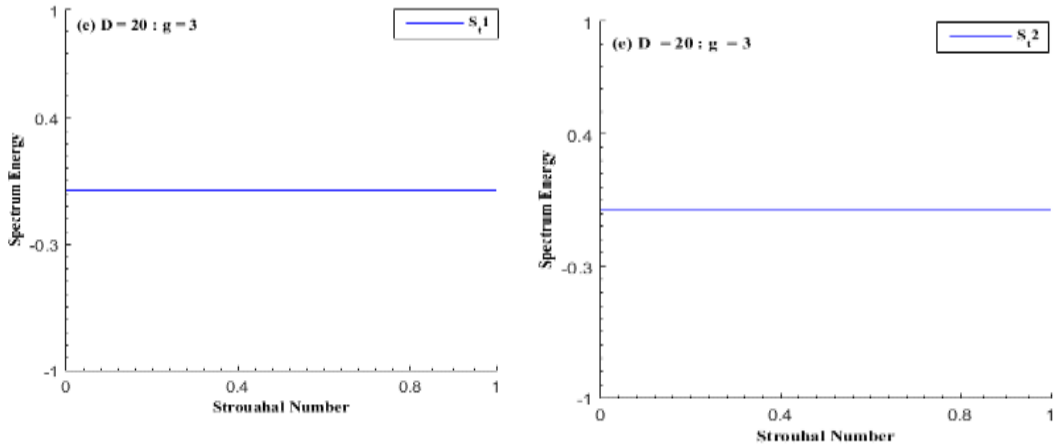

Fig 5(e) Strauhal number for SF flow regime at Re = 1

iv). Fully developed vortex shedding flow regime (FDVS)

The fourth and final observed flow regime is the fully developed vortex shedding flow (FDVS). In the present study, this flow is observed at (D, g) = (20, 5), (20, 6), (25, 5), (25, 6), (30, 5), (30, 6), (35, 6) , (35, 6), (40, 6) and (40, 6). For discussion, several cases of vorticity contour graphs are illustrating this flow regime and shown in Fig 5(a-c), providing a clear representation of this phenomenon. The vortex generation mechanism fully develops in round or oval shapes, maintaining the same size between C1 and C2, as well as in the wake behind the downstream cylinder at larger gap spacing's. It is also noted that the generated vortices exhibit alternate shedding in the wake behind the downstream cylinder, which indicates the presence of the Von-Karman vortex street (see Fig 6 (a-c)). As the gap spacing between the two unequal-sized cylinders C1 and C2 increases, the phenomenon becomes more pronounced. Because the cylinders have more space to generate the vortices at these larger gaps. This phenomenon was reported by Manzoor et al. (2016) for unequal-sized cylinders and by Manzoor et al. (2023). Due to the stagnation point, the fourth observed flow regime exhibits the maximum pressure at the front surface of the upstream cylinder (see Fig 6 (d, e, f)). At the largest gap spacings between C1 and C2, there is a significant reduction in pressure, which is not constant. In most of the computational domain, pressure is negligible, except at the front sides of both cylinders, where it reaches its highest values, resulting in a well-defined form of fully developed vortex shedding. In Fig 6 (d-f), the temporal variations of the drag coefficient (C_d1) and lift coefficient (C_l1) at larger gap spacings (g = 5 & 6) for upstream cylinder sizes D = 20, 25, 30, 35 and 40 exhibit periodic behavior for both the upstream and downstream cylinders in this flow regime. The periodic behavior indicates unsteady flow, which suggests the presence of vortices in the gap between the cylinders and in the wake behind the downstream cylinder throughout the computational domain. From the drag coefficient graphs, it is evident that the amplitude of $C_d1$is much greater than that of C_d2, which is due to the larger gap spacing between the two inline unequal-sized cylinders. Similarly, the time analysis of the lift coefficient graphs at larger gaps shows sinusoidal oscillations, with C_l2 exhibiting a greater amplitude than C_l1. This sinusoidal behavior reflects the mechanism of alternate vortex shedding throughout the channel. Fig 6(g-i) presents the spectral analysis plots of the lift coefficients at D = 20- 40 along with g = 5 & 6 for the final flow pattern. The Strouhal number graphs show a prominent, long primary peak along with multiple secondary peaks for the two unequal-sized cylinders at these largest gaps. It is observed that the Strouhal number for the upstream cylinder is larger than for the downstream cylinder due to the greater size of C1 compared to C2.

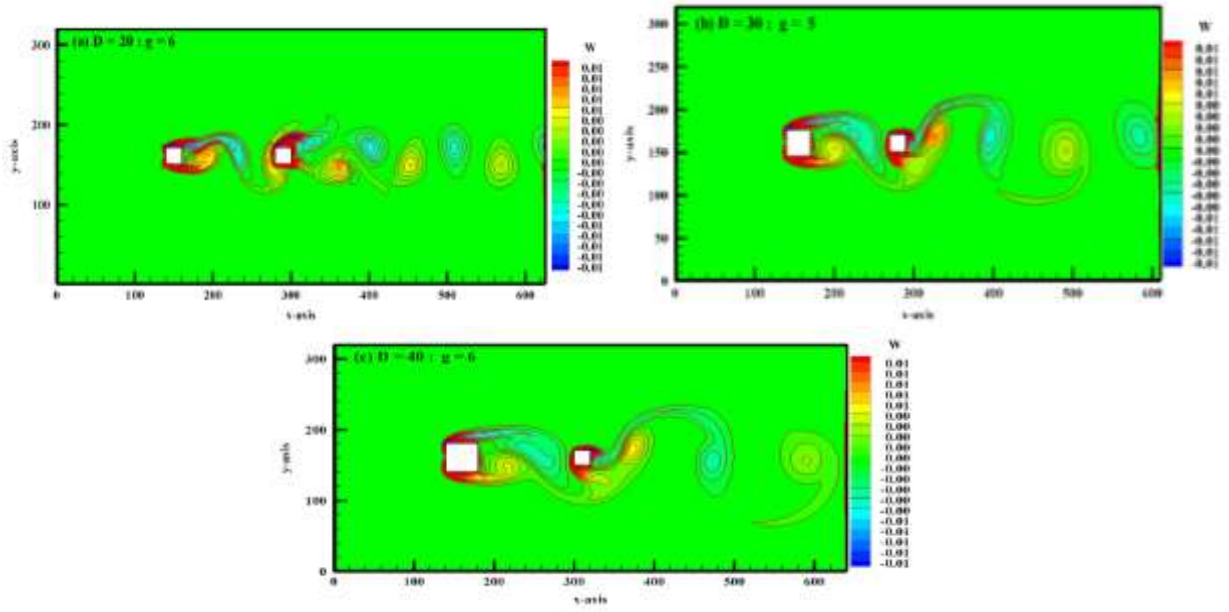

Fig 6 (a, b, c). Vorticity contour visualization for FDVS flow regime at Re = 150

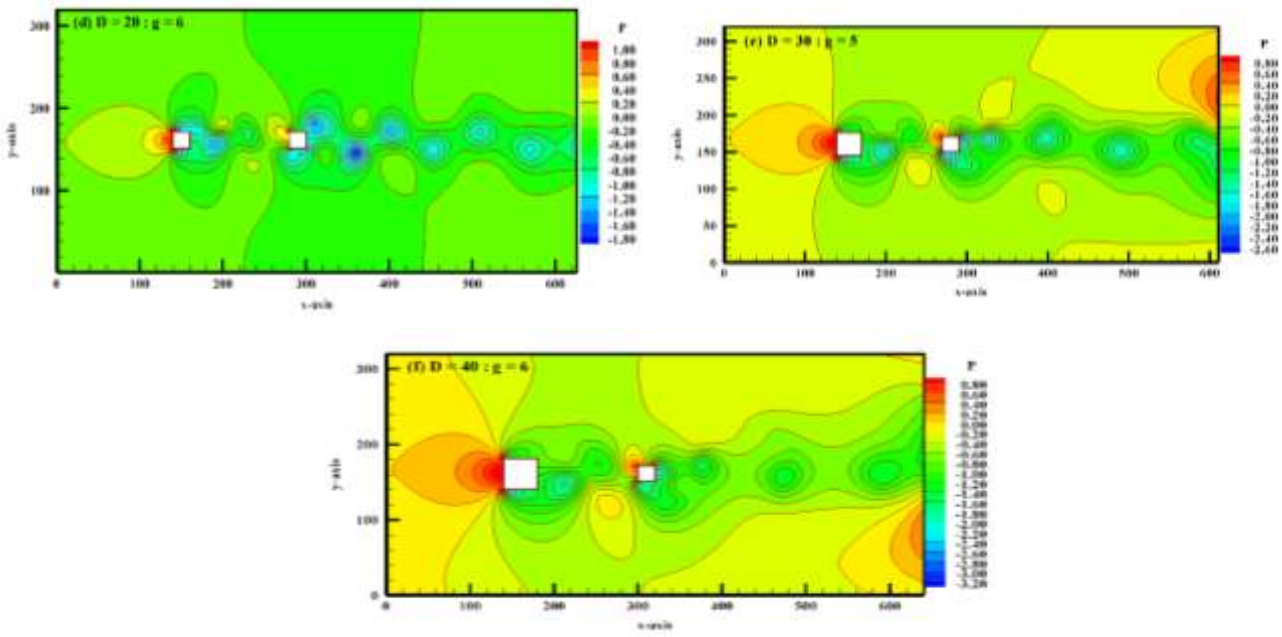

Fig 6 (d, e, f). Pressure contour visualization for FDVS flow regime at Re = 150

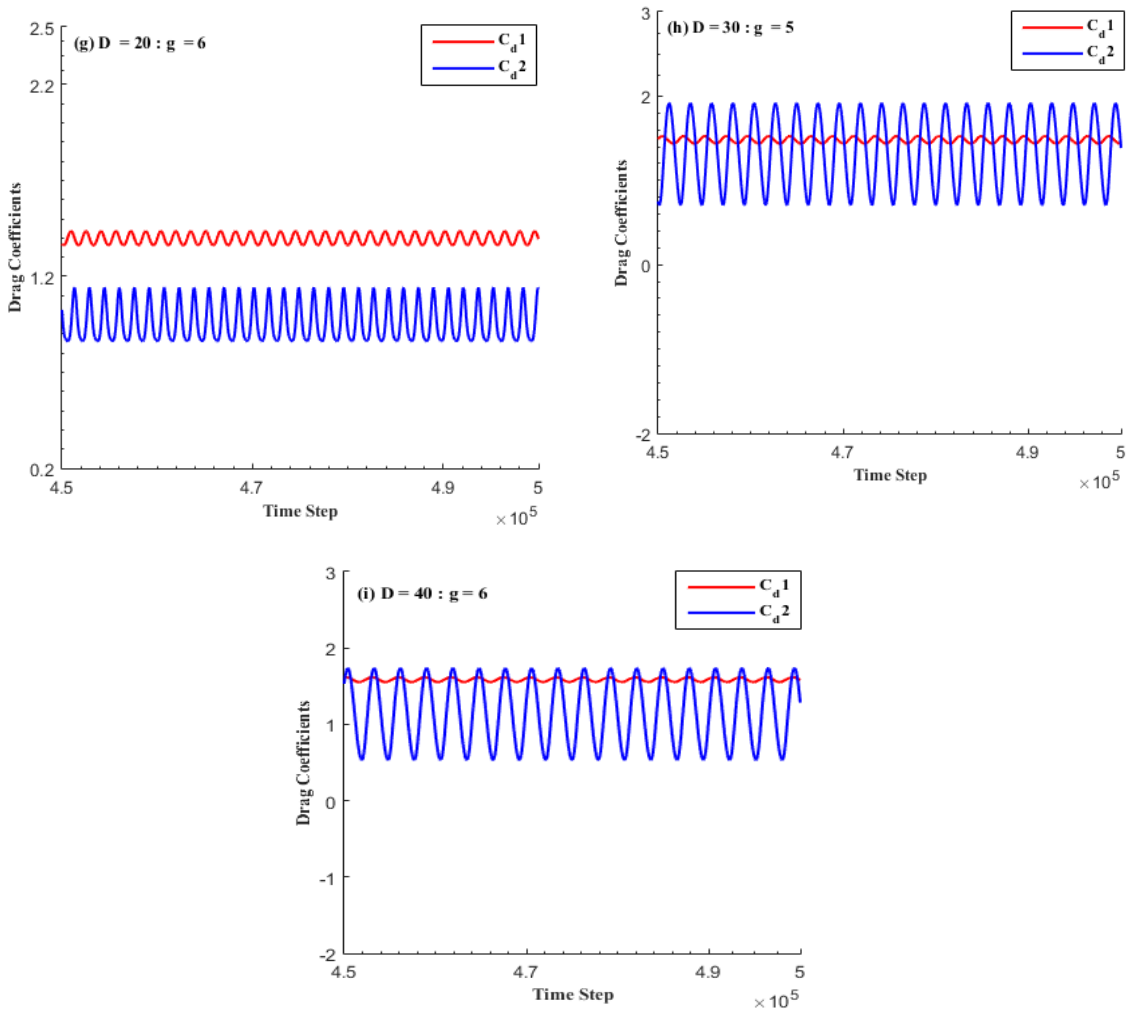

Fig 6 (g, h, i). Drag coefficient for FDVS flow regime at Re = 150.

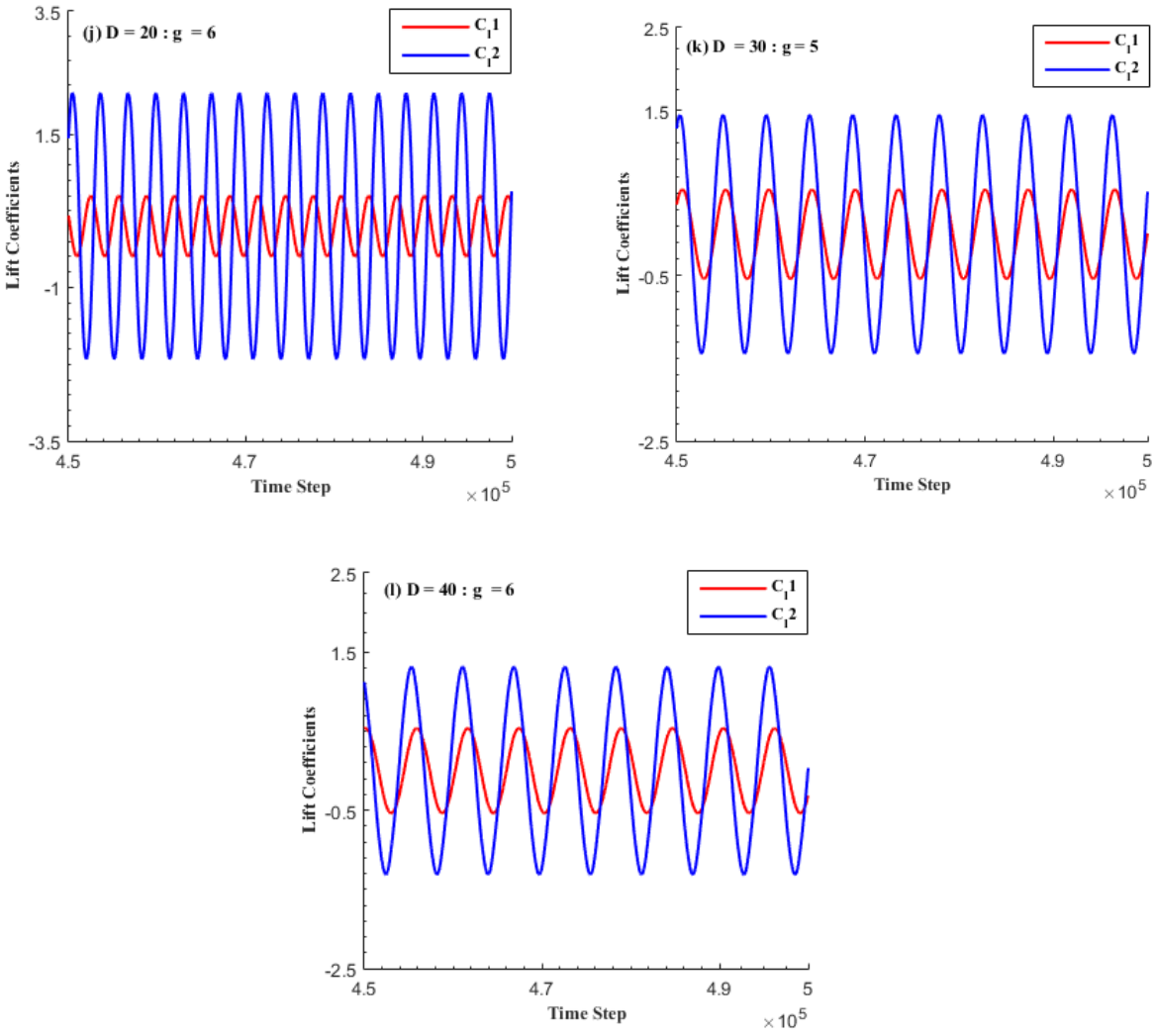

Fig 6 (j, k, l). Lift coefficient for FDVS flow regime at Re = 150.

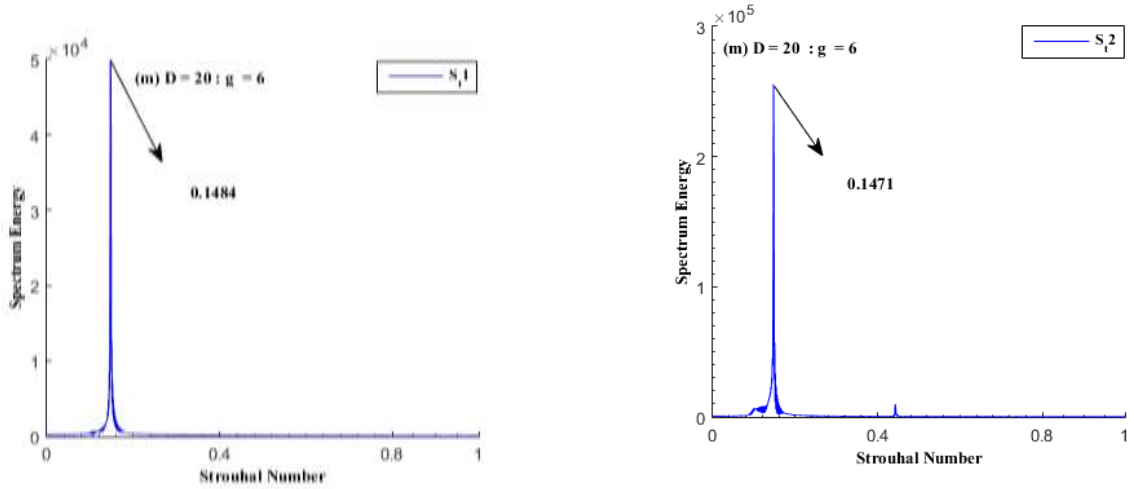

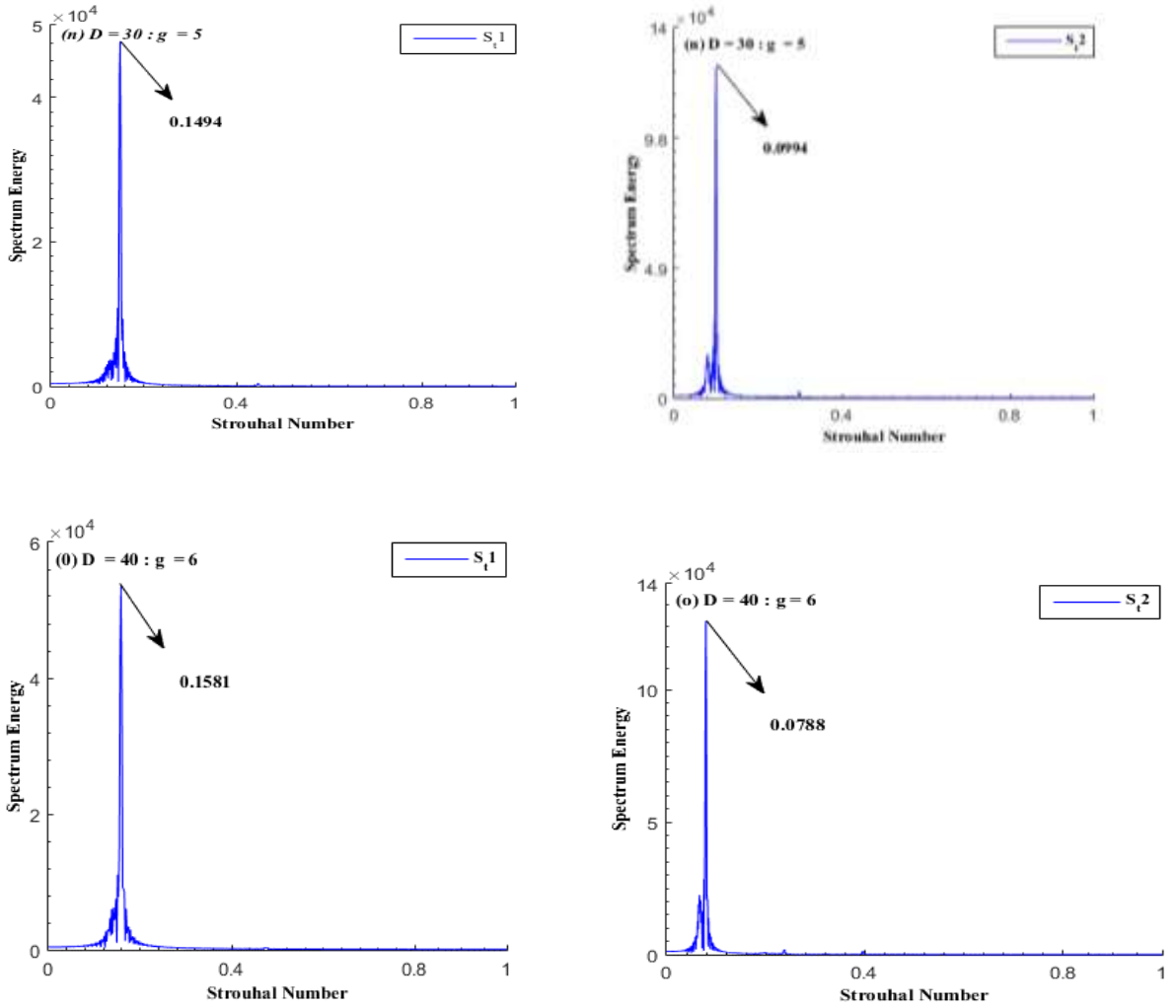

Fig. 6 (m, n, o). Strouhal number for FDVS flow regime at Re = 150.

5.2 Force Statistics

The two-dimensional numerical simulation is conducted by using the Lattice Boltzmann technique to compute fluid parameters such as C_{dmean}, C_{drms}, C_{lrms}, S_t for cylinders C1 and C2 as illustrated in Fig 7. This study is conducted to observe the impact of varying gap spacing and the size of the upstream cylinder within the ranges $0.5 \leq g \leq 6$ and $20 \leq D \leq 40$ on the flow mechanism behind two unequal-sized inline square cylinders. For the first cylinder C1, the mean drag coefficients $C_{dmean}1$ at D = 20 - 40 shows a slight decrease at g =1d−4d with a notable increase at g = 5 & 6. The maximum value of $C_{dmean}1$ is 1.5184 at the largest upstream cylinder size and gap spacing, (D, g) = (40, 6d. At this value, the flow regime is fully developed vortex shedding flow (FDVS) for C1. For the second cylinder C2, the mean drag coefficient (C_{dmean} 2) drops to negative values at upstream cylinder sizes D = 20, 25, and 30 due to the effect of thrust. However, at D = 35 & 40, $C_{dmean}2$ remains negative at g = 0.5d−5d, then suddenly it becomes positive with g = 5d & 6d, where its value rises at D = 20, 25 & 30. It is also observed that at D = 35 & 40 only g = 6d gives positive values. Maximum magnitude of $C_{dmean}2$ is obtained at D = 25 and g = 6, which is 1.6531.

The root mean square value of the drag coefficients ($C_{drms}1$) for the first cylinder is shown in Fig 7. A minor reduction is observed in $C_{drms}1$at D = 20, 30 & 40 with gap spacings, g =1−4, while a small increase is noted at D = 25 and g = 1 – 4. For the case of the upstream cylinder C1 at D = 35, $C_{drms}1$shows a slight increase at g = 1 & 2.5, followed by a decline from g = 3 & 4. Identical numerical values of $C_{drms}1$are observed for certain combinations of D and g, such as (D, g) = (20, 5), (20, 6), (25, 1), (25, 1.5), (25, 2.5), (35, 1.5), (35, 2) and (40, 1), (40, 1.5). An increasing trend in $C_{drms}1$is noted at (20,5), (25, 5), (30, 5), (30, 6), (35, 5), (35, 6) and (40, 5) with a small reduction observed in C_{drms} values of C1 at D = 25 & 40 with g = 6, where flow mode is fully developed vortex shedding flow. The highest value of $C_{drms}1$ is observed at (D, g) (30, 6) which is 0.764, while the smallest value is noted at (D, g) = (25, 0.5). Similarly, $C_{drms}2$ for the second cylinder is illustrated in Fig 7. For D = 20, $C_{drms}2$ isincreases with g = 1 and 1.5. Due to vortex generation as a single bluff body flow regime but decreases at g = 2 due to reattachment of shear layer flow regime. Afterward, the value of $C_{drms}2$ rises again from g = 2.5 to 5. For D = 25, 30 & 40, root mean square values of drag coefficients for C2 shows a minor increasing behavior within the range of g = 0.5 to 4. Abrupt high increases in $C_{drms}2$are observed at D = 20, 25, 30 & 40 at g = 5 and is representing increasing behavior at (D, g) = (25,6). The maximum value of $C_{drms}2$ is obtained at (D, g) = (30,6), which is 0.9484.

The root means square values of the lift coefficients for both cylinders C1 and C2 are shown in Fig 7. For the first cylinder, C_{lrms} value decreases for the flow behind two unequal-sized cylinders aligned with cylinder size D =20 and 30 at gap spacing g = 1 to 1.5, where the flow regime is shear layer reattachment and approaches to zero at g = 3d. Afterward, $C_{lrms}1$ increases at value of (D, g) = (20, 4) & (20, 5) and remains constant at g = 6 due to fully developed vortex shedding. For D = 25, $C_{lrms}1$ decreases from g = 1 to 2 but remains similar at g = 2.5. A rise is seen from g = 3 to 5, with a reduction at g = 6. For D = 30, $C_{lrms}1$ fluctuates from g = 3 to 6. For D = 35 $C_{lrms}1$ decreases from g = 1 to 1.5 and remains the same at g = 2. A decrease in $C_{lrms}1$ is observed at D = 40 from g = 1 to 3 and an increase from g = 4 to 6 is observed. The greatest value of $C_{lrms}1$ is obtained at (D, g) = (35,6), which is 0.3359. Similarly, values of $C_{lrms}2$ are illustrated in Fig 7. For the second cylinder, C_{lrms} values decreases from g = 1 to 3 at D = 20 and increases at g – 4 to 6. For D = 25, the value of $C_{lrms}2$ is similar at g = 1 to 2.5 and increases from g = 3 to 6. For D = 30 & 35 and g = 1 to 6, mixed trend is observed in the values of $C_{lrms}2$. For D = 40, $C_{lrms}2$ increases from g = 1 to 5, then decreases at g = 6. The maximum value of $C_{lrms}2$ is obtained at (D, g) = (20,5) that is 0.3972.

The Strouhal number values for both cylinders are shown in Fig 7. For the first cylinder, S_t increases with gap spacing g = 0.5 to 2 and remains relatively stable for g = 3 to 6. For D = 25, S_t decreases from g = 1 to 4 and remains constant at g = 5 & 6d. But for D = 30, 35 and 40, mixed trend in values of S_t is noticed at g = 1 to 6. The maximum value S_t for C1 is obtained at (D, g) = (25,6) and it is 0.7174. For the second cylinder C2, the values of Strouhal number shows a decreasing trend from g = 0.5 to 2 at D = 20, followed by a small increase at g = 2.5 to 6. For D = 25, St decreases from g = 1 to 4, then increases at g = 5 and 6. For D = 30 and 35, S_t decreases from g = 1 to 4, then shows a minor increase from g = 5 to 6. While for D = 40, S_t decreases from g = 1 to 3 and remains constant from g = 4 to 6. The highest value of S_t2 is obtained at (D, g) = (25,6).

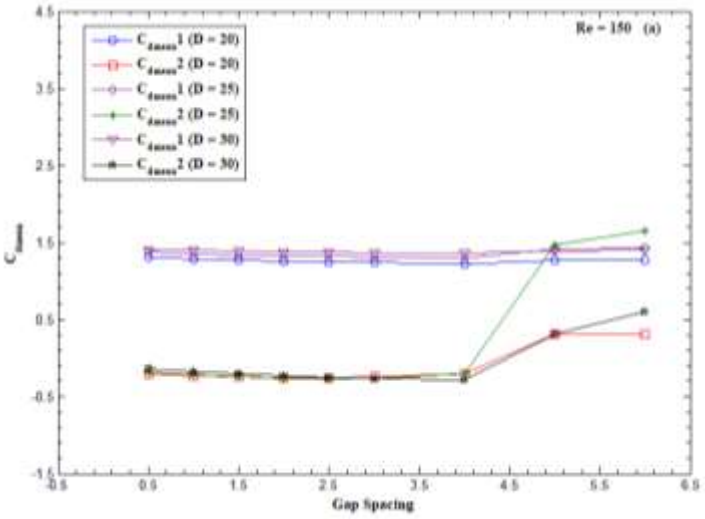

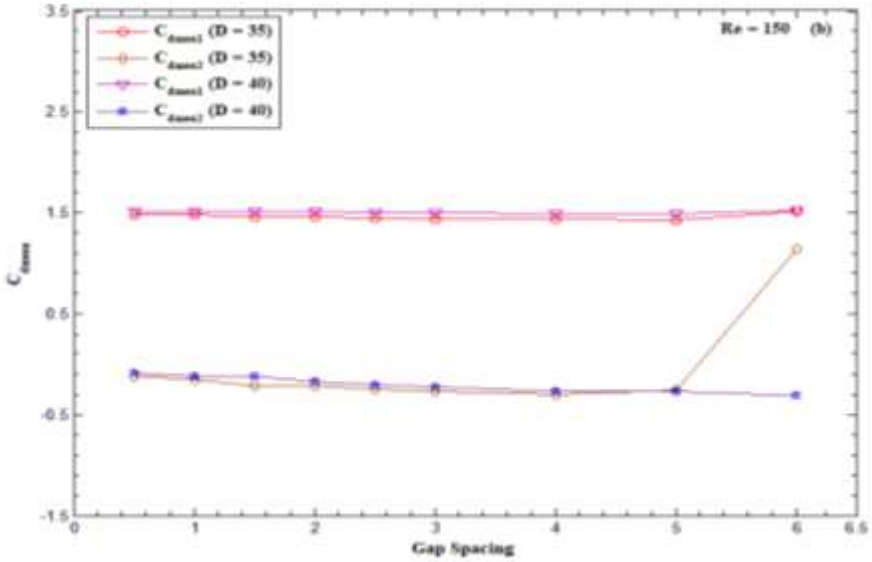

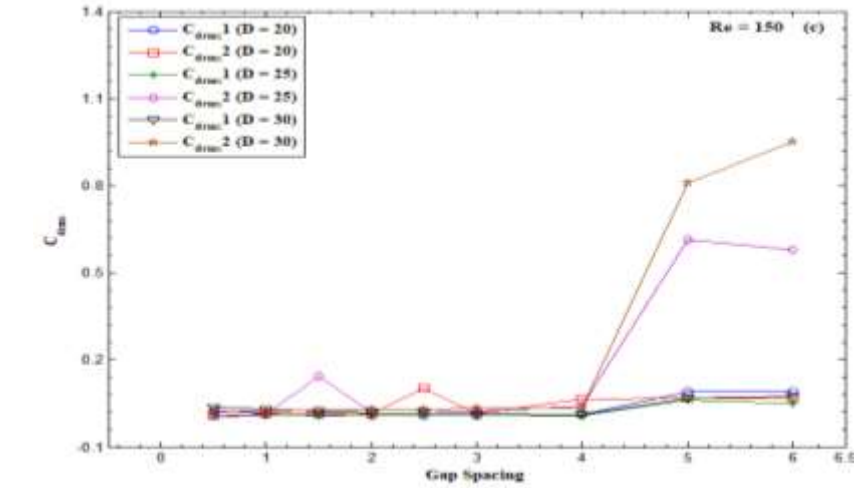
Re = 150 (c)
$C_{drms}1$ (D = 20)
$C_{drms}2$ (D = 20)
$C_{drms}1$ (D = 25)
$C_{drms}2$ (D = 25)
$C_{drms}1$ (D = 30)
$C_{drms}2$ (D = 30)
C_{drms}
Gap Spacing

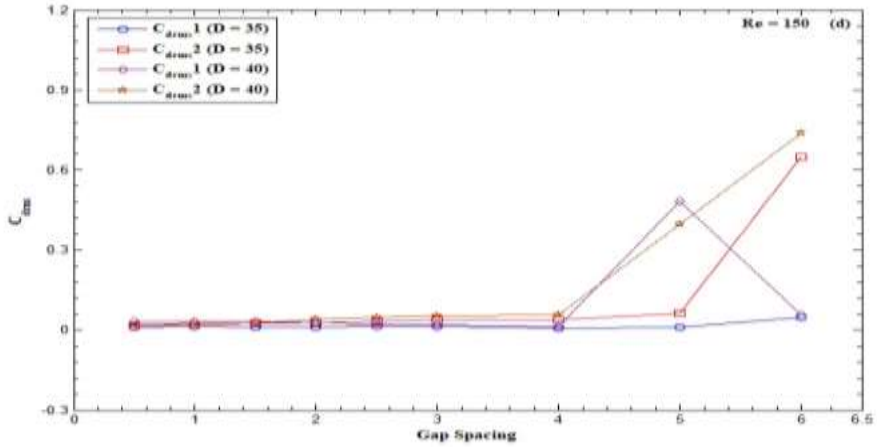
Re = 150 (d)
$C_{drms}1$ (D = 35)
$C_{drms}2$ (D = 35)
$C_{drms}1$ (D = 40)
$C_{drms}2$ (D = 40)
C_{drms}
Gap Spacing

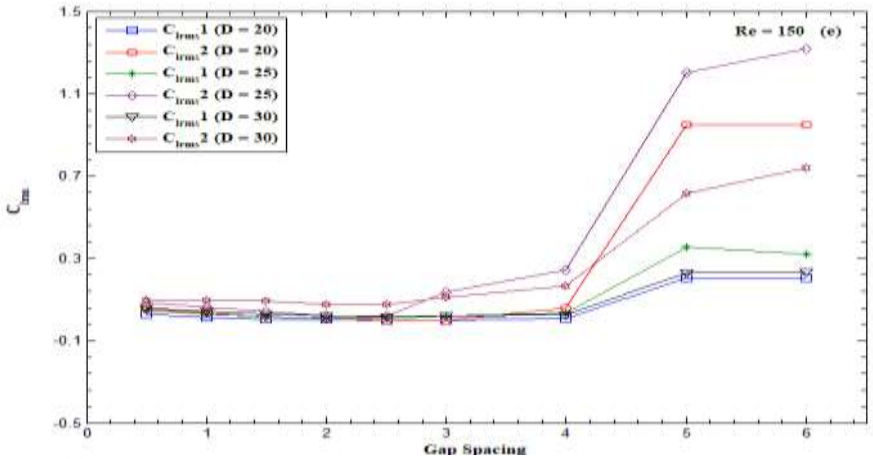
Re = 150 (e)
$C_{lrms}1$ (D = 20)
$C_{lrms}2$ (D = 20)
$C_{lrms}1$ (D = 25)
$C_{lrms}2$ (D = 25)
$C_{lrms}1$ (D = 30)
$C_{lrms}2$ (D = 30)
C_{lrms}
Gap Spacing

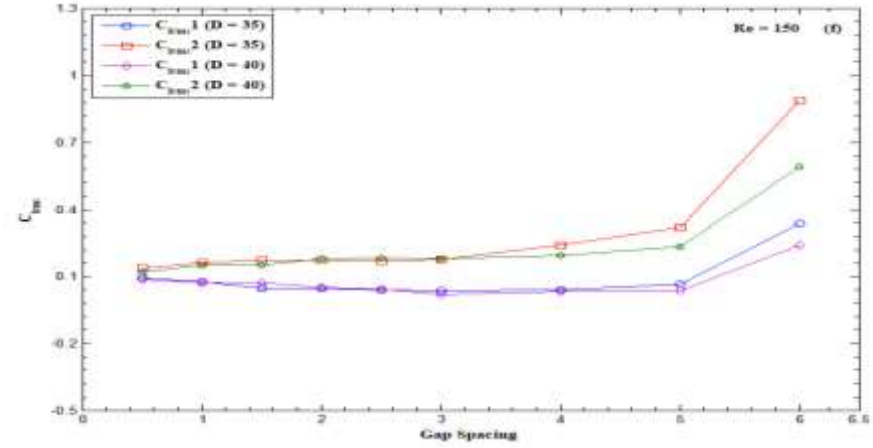
Re = 150 (f)
$C_{lrms}1$ (D = 35)
$C_{lrms}2$ (D = 35)
$C_{lrms}1$ (D = 40)
$C_{lrms}2$ (D = 40)
C_{lrms}
Gap Spacing

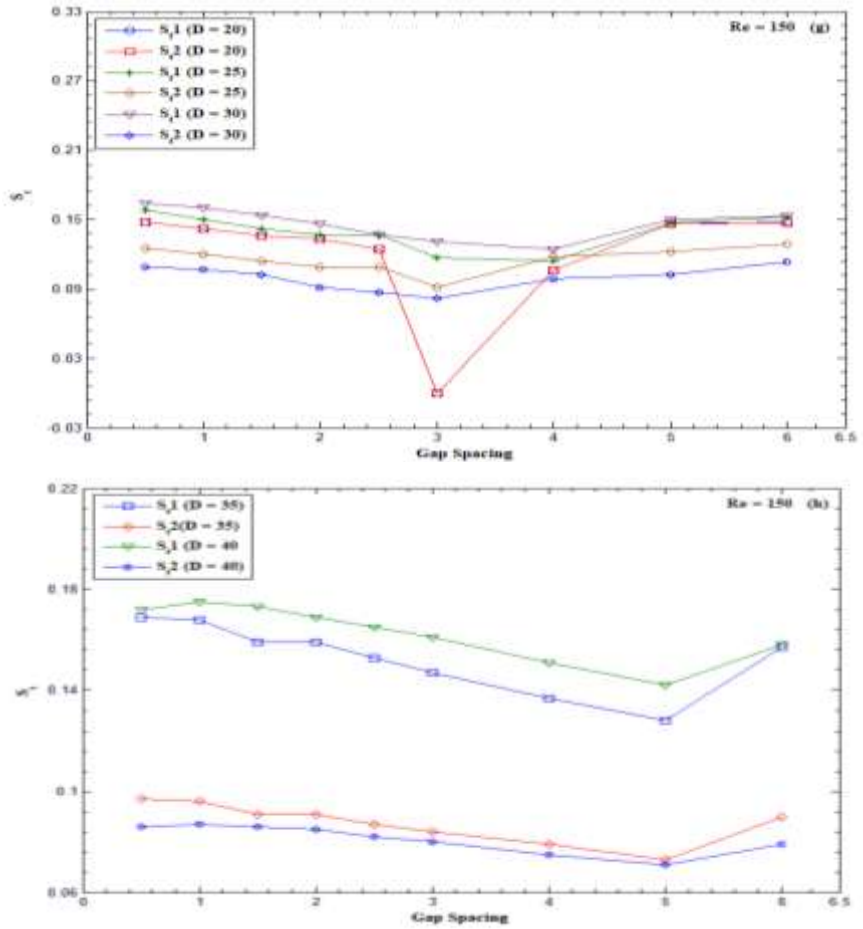

Fig .7 (a – h) Physical parameters for the flow around two inline un- equal size square cylinders with various gap spacing at Re = 150.

6. **Conclusions**:

Two-dimensional (2-D) numerical simulations have been conducted to examine the flow behavior influenced by various sizes of the upstream cylinder (D = 20, 25, 30, 35, and 40) while maintaining a fixed size for the downstream cylinder (d = 20). The Reynolds number was kept constant at Re = 150, with varying gap spacings between the two cylinders ranging from g = 0.5 to 6. The numerical technique used is the Lattice Boltzmann Method. Initially, different simulations were performed with varying upstream and downstream distances and channel heights to determine the most appropriate computational domain. A grid independence study was then conducted to identify the suitable grid point, with d = 20 being found as the most accurate for the present problem. Subsequent simulations for the selected problem revealed the following outcomes:

1. Four distinct types of flow regimes were examined for various diameters of the upstream cylinder (C1) and gap spacings, categorized as:
   - Single bluff body flow regime (SBB)
   - Shear layer reattachment flow regime (SLR)
   - Steady flow regime (SF)
   - Fully developed vortex shedding flow regime (FDVS)
2. Significant pressure variations were observed near the wake region and the surroundings of both cylinders. Maximum pressure was recorded on the front surface of the upstream cylinder (C1), while pressure on the rear corners dropped to negative values. The varying pressure distribution, including negative values, was attributed to the effects of shear layers and was not uniform throughout the computational domain.
3. For the largest size of the first cylinder D = 40 with a gap spacing of g = 6, the mean drag coefficients (C_{dmean}) for C1 reached its maximum value of 1.5184. The highest value of $C_{dmean}2$ was observed at (D, g) = (25, 6), which was 1.6531, corresponding to the Fully developed vortex shedding (FDVS) flow regime.
4. For the downstream cylinder (C2), the mean drag coefficient showed negative values at various (D, g) configurations due to the effect of thrust. Notable instances include (D, g) = (20, 0.5), (20, 1), (25, 0.5), and (30, 0.5), among others.
5. The highest numerical value of the root mean square drag coefficients (C_{drms}) for the first cylinder was observed at (D, g) = (30, 6), with a value of 0.764 under the FDVS regime. The lowest value was recorded at (D, g) = (25, 0.5) within the SBB regime. Similarly, for C2, the maximum C_{drms} was observed at (D, g) = (30, 6), with a value of 0.9484.
6. The root mean square lift coefficients for cylinder C1 dropped to zero at g = 3d and D = 20. The maximum C_{lrms} for C1 was recorded at (D, g) = (35, 6), with a value of 0.3359. For cylinder C2, the highest C_{lrms} was observed at (D, g) = (25, 6), with a value of 1.3159.

7. The study found that the magnitude of the Strouhal number for C1 was greater than for C2, attributed to the larger size of C1. The highest values were $S_t1 = 0.1581$ and $S_t2 = 0.078$, observed at $D = 40$ with $g = 6$.
8. The investigation revealed that the size of the upstream cylinder and the gap spacing between the two cylinders significantly affect the flow regimes and mechanisms. The findings from this study may be useful for optimizing structural arrangements.

7. References:

1. Chapmann, S., & Cowling, G. T. (1970). *Mathematical theory of non-uniform gases* (3rd ed.). Cambridge University Press.
2. Sakamoto, H., Haniu, H., & Obata, Y. (1987). Fluctuating forces acting on two square prisms in tandem arrangement. *Journal of Wind Engineering and Industrial Aerodynamics, 26*(1), 85-103.
3. Chiu, A. Y. W., & Ko, N. W. M. (1995). Bistable flow of two unequal square cylinders in various staggered arrangements. In *Twelfth Australian Fluid Mechanics Conference* (pp. 829-842). The University of Sydney.
4. Ko, N. W. M., Wong, P. T. Y., & Leung, R. C. K. (1996). Interaction of flow structures within bistable flow behind two circular cylinders of different diameters. *Journal Name, 12*(1), 33-44.
5. Gallivan, A. M., Noble, D. R., Georgia, G. J., & Buckius, O. R. A. (1997). An evaluation of the bounce-back boundary condition for Lattice Boltzmann simulations. *International Journal for Numerical Methods in Fluids, 25*(3), 249-263.
6. Guo, Z., Shi, B., & Wang, N. (2000). Lattice BGK model for incompressible Navier-Stokes equations. *Journal of Computational Physics, 165*, 288-298.
7. Dalton, C., Xu, Y., & Owen, C. J. (2001). The suppression of lift on a circular cylinder due to vortex shedding at regime Reynolds number. *Journal of Fluid and Structures, 15*, 617-628.
8. Zhang, H. J., & Zhou, Y. (2001). Effect of unequal cylinder spacing on vortex streets behind three side-by-side cylinders. *Physics of Fluids, 13*, 3675-3686.
9. Kang, S. (2003). Characteristics of flow over two circular cylinders in a side-by-side arrangement at low Reynolds numbers. *Physics of Fluids, 15*(9), 2486-2498.
10. Dazhi, Y., Renwei, M., Luo, L. S., & Wei, S. (2003). Viscous flow computations with the method of lattice Boltzmann equation. *Journal of Programic Aerospace Science, 39*(5), 329-367.
11. Zhou, L., Cheng, M., & Hung, K. C. (2005). Suppression of fluid force on a square cylinder by flow control. *Journal of Fluids and Structures, 21*, 151-167.
12. Wolf-Gladrow, D. (2005). *Lattice-gas cellular automata and lattice Boltzmann models: An introduction*. Springer.
13. Agrawal, A., Djenidi, L., & Antonia, R. A. (2006). Investigation of flow around a pair of side-by-side square cylinders using the lattice Boltzmann method. *Computers & Fluids, 35*(10), 1093-1107.
14. Sukop, M. C., & Thorn, D. T. (2007). *Lattice Boltzmann modelling: An introduction for geoscientists and engineers*. Springer.
15. Guo, H., Liu, L. S., Luo, S. C., & Xu, K. (2008). A comparative study of the LBE and GKS methods for 2D near incompressible laminar flows. *Journal of Computational Physics, 227*(10), 4955-4976.
16. Lee, K., & Yang, K. S. (2009). Flow patterns past two circular cylinders in proximity. *Computers & Fluids, 38*(4), 778-788.
17. Gao, Y. Y., Yu, D., Tan, S., Yang, X., & Hao, Z. (2010). Experimental study on near wake behind two side-by-side cylinders of unequal diameter. *Fluids Dynamics Research, 42*(5).
18. Mohamad, A. A. (2011). *Lattice Boltzmann method: Fundamentals and engineering applications with computer codes*. Springer.
19. Yen, S. C., & Liu, J. H. (2011). Wake flow behind two side-by-side square cylinders. *International Journal of Heat and Fluid Flow, 32*(3), 41-51.
20. Sohankar, A. (2012). A numerical investigation of the flow over a pair of identical square cylinders in a tandem arrangement. *International Journal for Numerical Methods in Fluids, 70*(10), 1244-1257.
21. Gao, Y. Y., Wang, X. K., & Tang, S. K. (2012). Numerical study of two side-by-side cylinders with unequal diameters at low Reynolds numbers. *Earth and Environmental Science, 15*, 1-12.
22. Bao, Y., Wu, Q., & Zhou, D. (2012). Numerical investigation of flow around an inline square cylinder array with different spacing ratios. *Computers & Fluids, 55*, 118-131.
23. Luo, S. C., & Gan, T. L. (2016). Flow past two tandem circular cylinders of unequal diameter. *Journal Name, 96*(953), 105-114.
24. Manzoor, R., Islam, S.-U. L., Abbasi, S. W., & Parveen, S. (2016). Variation of wake patterns and force coefficients of the flow past square bodies aligned inline. *Journal of Mechanical Science and Technology, 30*(4), 691-704.
25. Islam, S.-U. L., Shigri, S. H., Ying, Z. C., & Akbar, T. (2017). A computational study of flow past three unequal-sized square cylinders at different positions. *AIP Advances, 7*, 035303.
26. Hamid, R., Islam, S.-U. L., Abbasi, W. S., & Nazeer, G. (2019). A numerical study for flow around three-square cylinders in triangular arrangement. *Iranian Journal of Science and Technology, 44*, 229-246.
27. Skonecki, M., & Buick, J. M. (2023). Numerical study of flow around two circular cylinders in tandem, side-by-side, and staggered arrangements. *Journal of Fluids, 8*(5), 148.
28. Manzoor, R., Islam, S.-U. L., Jalil, M., Akhtar, Y., Ahmad, A., & Kalsoom, S. (2024). Fluid structure interaction problem for flow past three unequal-sized square cylinders at different Reynolds numbers. *Physics of Fluids, 36*, 044107.